Inflow Turbulence Generation Methods

Xiaohua Wu

Department of Mechanical and Aerospace Engineering, Royal Military College of Canada, Kingston K7K 7B4, Ontario, Canada; email: Xiaohua.Wu@rmc.ca

Abstract

Research activities on inflow turbulence generation methods have been vigorous over the past quarter century, accompanying advances in eddy-resolving computations of spatially developing turbulent flows with direct numerical simulation, large-eddy simulation (LES), and hybrid Reynolds-averaged Navier-Stokes–LES. The weak recycling method, rooted in scaling arguments on the canonical incompressible boundary layer, has been applied to supersonic boundary layer, rough surface boundary layer, and microscale urban canopy LES coupled with mesoscale numerical weather forecasting. Synthetic methods, originating from analytical approximation to homogeneous isotropic turbulence, have branched out into several robust methods, including the synthetic random Fourier method, synthetic digital filtering method, synthetic coherent eddy method, and synthetic volume forcing method. This article reviews major progress in inflow turbulence generation methods with an emphasis on fundamental ideas, key milestones, representative applications, and critical issues. Directions for future research in the field are also highlighted.

1. INTRODUCTION

The ever-increasing prevalence of computational fluid dynamics (CFD) over the past half century as a tool to predict flow device performance and to investigate transition and turbulence physics owes a significant part to the tremendous progress in eddy-resolving simulation techniques, namely direct numerical simulation (DNS), large-eddy simulation (LES), and hybrid Reynolds-averaged Navier-Stokes (RANS)-LES. These techniques capture, to varying degrees of accuracy, the stochastic characteristics of turbulent eddies for a wide range of scales as well as their statistical spatial and temporal coherence. Early work on LES was reviewed by Rogallo & Moin (1984), followed by subsequent reviews on DNS by Moin & Mahesh (1998) and on hybrid RANS-LES by Spalart (2009).

The duality of simultaneous randomness and coherence associated with turbulent eddying motion is a result of the particular nonlinearity of the Navier-Stokes equation system and poses challenges to eddy-resolving simulation techniques. The challenge is particularly pronounced at the inflow boundary of spatially developing turbulence simulations for which the accurate prescription of the incoming turbulent eddies as a function of time is a prerequisite to obtaining the unsteady solution in the interior of the domain. Logically, this prescription can be obtained if the turbulent eddying motion through the inflow plane can be considered as the solution of the Navier-Stokes equations in the interior of an auxiliary computational domain. The circularity of the procedure can be overcome if turbulence in the auxiliary domain is spatially homogeneous in the streamwise direction along which the strictly periodic boundary condition is applicable (strong recycling); another possibility is that the turbulence in the auxiliary domain is a result of an accurately captured clean laminar-to-turbulent transition process with minimal downstream footprints (Wu et al. 2014, 2015). Alternatively, an approximation to this prescription may be constructed synthetically by imposing coherence constraints on a random number field or by adding random perturbations to a deterministic coherent field (synthetic turbulence), with the understanding that such an approximation is not a solution of the Navier-Stokes equation system.

Both the importance and difficulty associated with inflow turbulence generation in spatially developing simulations were recognized by early researchers using eddy-resolving techniques. The issue can be circumvented by limiting the simulation scope to flows with streamwise homogeneity and devoid of the inflow-outflow type of boundaries, as in the fully developed turbulent channel simulation of Moin & Kim (1982) (see Rogallo & Moin 1984 for a full account of the early LES and DNS work on temporally developing turbulent flows with at least two spatially homogeneous directions). As a result, the problem of inflow turbulence generation remained virtually untouched until the early 1990s. Lee et al. (1992) explicitly highlighted this issue in their DNS of spatially decaying compressible homogeneous isotropic turbulence (HIT). The field received a strong impetus in the mid- to late 1990s when multiple simultaneous DNS and LES attacks on complex turbulent boundary layers brought into focus the issue of generating a turbulent incompressible zero-pressure-gradient smooth flat-plate boundary layer (ZPGSFPBL) for the inflow condition (Lund & Moin 1996, Le et al. 1997, Na & Moin 1998, Wu & Squires 1998). Entering the new millennium, as DNS and LES continued their expansion into aerodynamics, atmospheric science, computational wind engineering (CWE), and computational aeroacoustics (CAA), the need for accurate upstream baselines of a turbulent compressible ZPGSFPBL and a turbulent zero-pressure-gradient rough surface flat-plate boundary layer (ZPGRFPBL) has both broadened and deepened the field of inflow turbulence generation. In recent years, increased engineering applications of the hybrid RANS-LES methodology have added an extra dimension to this vibrant research field. This article reviews progress in inflow turbulence generation over the past quarter century and highlights the outstanding issues.

2. RECYCLING INFLOW TURBULENCE GENERATION

2.1. Strong Recycling Method

Laboratory CFD research on spatially developing flow usually, but not always, starts with an idealized, equilibrium (self-similar) upstream inflow condition that is free of extraneous perturbation factors. One then proceeds to examine the development of such a baseline state in space-time as it responds to imposed downstream nonequilibrium environmental variables or simply to the extension of the streamwise domain. The incoming stream approaching a standing normal shock wave in Lee et al. (1993) was time-dependent, unforced compressible HIT; the upstream flow discharging into a coaxial combustor in Pierce & Moin (2004) was a fully developed turbulent coaxial pipe flow; and the feed flow into an asymmetric planar diffuser in Wu et al. (2006) was a fully developed turbulent channel flow. Eddy-resolving approaches for computing these canonical equilibrium baselines are well established: Because they are statistically homogeneous in space along the directions without nonuniform mean shear, the computations make use of the strictly periodic boundary condition in such directions (Rogallo & Moin 1984, Moin & Mahesh 1998). The velocity vector fields of such baseline flows resolved using the strictly periodic condition in the streamwise direction are denoted as $\mathbf{u}_{sr}(\mathbf{x}, t)$, where the subscript denotes strong recycling.

In the strong recycling method of inflow turbulence generation, the temporal record of $\mathbf{u}_{sr}(\mathbf{x}, t)$ at one selected streamwise station x_{sl} of an auxiliary simulation is used to prescribe the velocity field at the inlet plane of the main spatially developing simulation, $\mathbf{u}(x_{in}, y, z, t) = \mathbf{u}_{sr}(x_{sl}, y, z, t)$. This seemingly simple procedure actually entails a number of subtleties. Obviously, for internal flows, the geometry of the plane $x = x_{sl}$ in the auxiliary periodic computation should be identical to that at $x = x_{in}$ in the spatial simulation. If the flow is unbounded in the transverse directions, this constraint may be relaxed by simply requiring the $x = x_{sl}$ plane to be no smaller than the $x = x_{in}$ inlet plane. A counterexample violating this constraint can be found in Kalitzin et al. (2003), which involved unphysical stacking of the same eddy stream in order to fill up the inflow plane. Additionally, Chung & Sung (1997) pointed out that both the grid resolution and Reynolds number of the auxiliary periodic computation and the main spatial computation should be identical (or at least comparable). Resolution matching poses a challenge when C- or O-type grids are used in the spatial simulation. Ordinarily, matching of the Reynolds number is straightforward. However, caution should be exercised when introducing HIT or similar types of unbounded baseline flows into a spatial computation with distinctly different length scales dictated by the geometry. In the HIT past a turbine cascade DNS of Wu and colleagues (Wu et al. 2009, Wu & Hickey 2012), two Reynolds numbers are involved: $Re_c = U_f c / \nu$, based on the blade cord c, and $Re_\lambda = u'_{rms} \lambda / \nu$, based on the Taylor microscale λ of the HIT. Although Re_c is absent in the auxiliary HIT simulation, its constraint should still be enforced in the generation of inflow turbulence. This can be achieved by matching the inlet turbulence intensity u'_{rms} measured in terms of the free-stream velocity U_f, λ measured in terms of c, and the kinematic viscosity ν.

A popular variant of the strong recycling method is to sweep along the streamwise direction of the auxiliary periodic simulation domain at one or multiple selected instants t_{se} by invoking Taylor's frozen turbulence hypothesis to acquire the inflow temporal sequence. Although the precise value of the convective velocity used in the hypothesis is difficult to determine, it is nevertheless often taken as the bulk velocity U_b for internal flow and the far-upstream velocity U_f for external flows. This is essentially equivalent to concatenating realizations of the auxiliary flow $\mathbf{u}_{sr}(\mathbf{x}, t_{se})$ at different instants of t_{se} into a long stream. Chung & Sung (1997) compared this variant with the original strong recycling method using the channel flow and reported negligible differences. When only a few t_{se} instants are used in the procedure, it is desirable to break the repetition of

$\mathbf{u}_{sr}(\mathbf{x}, t_{se})$ in the main spatial simulation by introducing random perturbations into the sequence. For baseline flows with both streamwise and spanwise homogeneity, this can be achieved by performing Fourier transform on $\mathbf{u}_{sr}(\mathbf{x}, t_{se})$ in the spanwise direction, slightly adjusting either the amplitude (amplitude jittering) or phase angle (phase jittering) using a random perturbation factor that is close to unity, and transforming back to the physical space. Chung & Sung (1997) found that amplitude jittering yields better performance than phase jittering because the resulting sequence preserves the resolved eddy structures, whereas phase jittering preserves the sampled statistics. Popular in the 1990s (Lee et al. 1993, Le et al. 1997, Mahesh et al. 1997, Na & Moin 1998), these jittering procedures have been used less often in recent years given the increased availability of disk space to store sufficiently long temporal sequences of $\mathbf{u}_{sr}(\mathbf{x}, t_{se})$.

Wu et al. (2014) concatenated a very long stream of HIT through the random permutation of 25 independent auxiliary HIT realizations, which provided inflow turbulence to their DNS of a ZPGSFPBL beneath mild free-stream turbulence. The resulting stream is much longer than required by the main spatial simulation. The mild free-stream HIT excites the ordered laminar-to-turbulent transition inside the boundary layer (a bypass transition in the narrow sense) and maintains excellent isotropic turbulence properties further downstream. Wu et al. (2015) used a similar random permutation of 50 independent fully developed turbulent pipe flow realizations as inflow to promote spatially developing pipe transition to turbulence. When two or more independent realizations of auxiliary periodic simulations are concatenated, the two-point correlation functions of the resulting stream near the concatenation interface may not be the same as those in the individual realizations. A remedy was proposed by Xiong et al. (2004) through the addition of a blending zone between the neighboring realizations, whose linear combination is used to construct the velocity fields in the blending zone. The length of the blending zone is adjustable, and the coefficients for the linear combination vary with spatial coordinates and are chosen empirically. Dilatation can also be minimized in the blending zone by solving a Poisson equation. Further development of the blending procedure was reported by Larsson (2009).

The strong recycling method relies on the streamwise periodicity of the auxiliary temporal simulation. This periodicity is passed on, not necessarily through the reuse and downstream convection of the database fields, to the main spatial simulation, resulting in mathematically consistent but physically unrealistic streamwise-repetitive features. Such spurious periodicity embedded in the strong recycling method was insightfully demonstrated by Nikitin (2007) using a spatially developing pipe flow in conjunction with a short streamwise-periodic auxiliary pipe. With the periodic turbulent pipe solution as the initial condition, the spatial simulation immediately establishes instantaneously repetitive flow patterns nearly identical to those of the instantaneous auxiliary flow. When the laminar parabolic velocity profile was used as the initial condition, the spatial simulation gradually established an instantaneously repetitive flow pattern. The deviation between this unphysical spatially repetitive solution and the periodic auxiliary solution grows exponentially with axial distance, but remains negligibly small near the outlet of their main simulation. The evidence presented in Nikitin (2007) reveals one substantial shortcoming that seems to be inherent to the strong recycling method: Spurious periodicity can arise spontaneously in the main spatial simulation through mechanism(s) other than the direct reuse and downstream convection of the periodic database fields. This artifact manifests itself more distinctively when the main spatial simulation is a simple streamwise extension of the auxiliary periodic temporal simulation. The concern may be alleviated when finite perturbation factors are present in the spatial simulation, such as changes in the geometry or surface roughness, or when the inlet turbulence is used only to promote downstream laminar-to-turbulent transition. In this sense, the strong recycling method, although certainly superior compared to synthetic methods, is still less accurate than extracting inflow turbulence from an accurate spatial transition simulation (Wu et al. 2014, 2015).

2.2. Weak Recycling Method

An important canonical case in modern fluid mechanics is the incompressible ZPGSFPBL, which is frequently used as the upstream baseline upon which downstream perturbation factors are imposed and the subsequent response monitored. Examples include the DNS calculations on a ZPGSFPBL encountering a downstream backward-facing step (Le et al. 1997) and on a ZPGSFPBL subjected to a downstream adverse pressure gradient (Na & Moin 1998). The inflow turbulence generation approaches in these studies made use of the temporal ZPGSFPBL statistics of Spalart (1988) but did not take advantage of his multiscaling idea for developing a general scheme.

Wu et al. (1995) presented a weak recycling method for inflow turbulence generation of the ZPGSFPBL by modifying and simplifying the temporal approach of Spalart (1988) for a spatial simulation. Assuming that the ZPGSFPBL flow scales with wall unit y^+ in the inner region and with y/δ in the outer region, they decomposed the instantaneous streamwise velocity signal at the inflow plane x_{in} and at one selected station x_{re} near the outlet as

$$u(x, \xi, z, t) = \langle u \rangle (x, \xi) + u'_{\mathrm{rms}}(x, \xi) u_{\mathrm{P}}(x, \xi, z, t), \tag{1}$$

where $\xi(y^+, y/\delta)$ is a composite distance variable that reduces to y^+ in the inner region and to y/δ in the outer region with a suitable blending function in between (Spalart 1988). At the beginning of a new time step $t + \Delta t$, the weakly periodic signal from the previous time step $u_{\mathrm{P}}(x, \xi, z, t)$ "at a location near the exit boundary of the computational domain is reintroduced at the inflow boundary" (Wu et al. 1995),

$$u(x_{\mathrm{in}}, \xi_{\mathrm{in}}, z, t + \Delta t) = \langle u \rangle (x_{\mathrm{in}}, \xi_{\mathrm{in}}) + u'_{\mathrm{rms}}(x_{\mathrm{in}}, \xi_{\mathrm{in}}) u_{\mathrm{P}}(x_{\mathrm{re}}, \xi_{\mathrm{in}}, z, t). \tag{2}$$

The wall-normal and spanwise velocity components are treated in an identical manner. Note that the decomposition is necessary only for these two selected streamwise stations. The simulation is still performed in the original Cartesian system. Wu et al. (1995) applied this weak recycling method to LES of a ZPGSFPBL developing in the momentum-thickness Reynolds number range $1{,}470 < \mathrm{Re}_\theta < 1{,}700$ and obtained reasonable comparisons with classical experimental data on mean and selected second-order and third-order statistics. The method was also applied by Lund & Moin (1996) in their LES study of a turbulent ZPGSFPBL encountering a downstream concave surface.

Along the same line of reasoning as in Wu et al. (1995), Lund et al. (1998) described a more formalized version of the weak recycling method, known as the LWS method. At x_{in} and x_{re}, they decomposed the instantaneous velocity vector signal as $\mathbf{u}(x, y, z, t) = \langle \mathbf{u} \rangle (x, y) + \mathbf{u}'(x, y, z, t)$ without introducing the new intermediate coordinate $\xi(y^+, y/\delta)$. The scaling role played by $\xi(y^+, y/\delta)$ in Wu et al. (1995) is accounted for by performing explicit inner and outer scaling on the velocity components directly. In other words, the scaling of the independent variable is replaced by the equivalent scaling on the dependent variable. Specifically, the fluctuating part of the inlet velocity field is prescribed as

$$\mathbf{u}'(x_{\mathrm{in}}, y_{\mathrm{in}}^+,\ z, t + \Delta t) = \frac{u_{\tau,\mathrm{in}}}{u_{\tau,\mathrm{re}}} \mathbf{u}'(x_{\mathrm{re}}, y_{\mathrm{in}}^+, z, t) \ \ \text{and} \ \ \mathbf{u}'\left(x_{\mathrm{in}}, \frac{y_{\mathrm{in}}}{\delta_{\mathrm{in}}}, z, t + \Delta t\right) = \frac{u_{\tau,\mathrm{in}}}{u_{\tau,\mathrm{re}}} \mathbf{u}'\left(x_{\mathrm{re}}, \frac{y_{\mathrm{in}}}{\delta_{\mathrm{in}}}, z, t\right) \tag{3}$$

for the inner and outer regions, respectively. In principle, the mean velocity components $\langle \mathbf{u} \rangle (x_{\mathrm{in}}, y)$ at the inlet of a ZPGSFPBL inflow generation simulation are less challenging and can be obtained through either the interpolation of classical experimental/numerical data or the application of an empirical correlation. They can also be acquired dynamically from the inflow generation simulation itself. In the LWS method, the inlet mean wall-normal velocity is scaled in the same way as the turbulent fluctuations, and the mean streamwise velocity component at the inlet is scaled with the

law of the wall for the inner region and the defect law for the outer region. The empirical relation $u_{\tau,\mathrm{in}}/u_{\tau,\mathrm{re}} = (\theta_{\mathrm{re}}/\theta_{\mathrm{in}})^{1/8}$ is invoked for estimating the scaling factor in Equation 3, where θ is the boundary layer momentum thickness. In the same spirit as the blending function for $\xi(y^+, y/\delta)$ in Wu et al. (1995), an empirical weighting function $W(y_{\mathrm{in}}/\delta_{\mathrm{in}})$ is used to blend the inner and outer regions and produce an instantaneous composite velocity profile at the inlet.

The spurious periodicity associated with the strong recycling method persists in ZPGSFPBL simulations using the weak recycling method (Simens et al. 2009, Lee & Sung 2011a). Simens et al. chose to locate the recycling plane significantly downstream from the inlet at $850\,\theta_{\mathrm{in}}$ to dampen the spatial spurious periodicity. They also pointed out that it is necessary to discard the results in the adjustment zone $0 < x < 300\,\theta_{\mathrm{in}}$. It is unclear if the decay rate for the strength of the spurious periodicity in the LWS weak recycling method is similar to that in the strong recycling of the pipe flow of Nikitin (2007). Positioning the recycling station far downstream, although beneficial for mitigating the spurious periodicity, can cause unintended errors in the flow structure given that the timescale and spanwise length scale at the recycling plane will be quite different from those at the inlet. Nevertheless, the procedure was deemed accurate and subsequently used in the statistical and structural investigations on the turbulent ZPGSFPBL itself by Jiménez et al. (2010) and Lee & Sung (2011b).

In many engineering CFD applications, an upstream turbulent ZPGSFPBL is often distorted by a downstream abrupt change in the surface geometry. For this type of problem, the LWS weak recycling method may be further simplified. Spalart et al. (2006) proposed to position the recycling station close to the inflow plane and to apply the outer scaling throughout the boundary layer given that the near-wall turbulence regenerates itself more quickly. They omitted the rescaling operation on the wall-normal velocity component and instead performed outer scaling only on the streamwise and spanwise velocity components. Spalart et al. also introduced a constant spanwise shift to disrupt the coherence between the recycling station and inlet plane. A similar shifting technique was adopted later by Jewkes et al. (2011) and Arolla & Durbin (2014).

Some authors reported that the initial condition affects whether the LWS weak recycling method can successfully establish a turbulent ZPGSFPBL and proposed elaborate remedy schemes (Ferrante & Elghobashi 2004, Liu & Pletcher 2006). Recent experience suggests that those complicated modifications are perhaps unnecessary with fine grid resolution (Simens et al. 2009, Jewkes et al. 2011, Lee & Sung 2011a). The LWS weak recycling method has also been extended to self-similar incompressible turbulent boundary layers under a favorable streamwise pressure gradient or weak adverse pressure gradient. For such flows, Araya et al. (2009, 2011) proposed to scale the wall-normal velocity fluctuation differently from the other two components by considering the growth effect of $U_f\,d\delta/dx$ (see also Araya et al. 2015). Wu & Squires (2000) applied the weak recycling method in their LES of the three-dimensional turbulent boundary layer over a rotating disk.

2.3. Extension of Weak Recycling to Compressible Boundary Layers

The compressible turbulent ZPGSFPBL is of fundamental importance in aeronautical fluid dynamics: It is the prototype for the flow over an aircraft wing and also the upstream baseline for many complex supersonic processes, such as shock wave and boundary layer interaction (SWBLI). As such, eddy-resolving simulations of the compressible ZPGSFPBL have received special attention from the aeronautical CFD community, starting from the coarse resolution and brute force attempt of Rai & Moin (1993). Shortly after the publications of Wu et al. (1995) and Lund et al. (1998), work began on extending the weak recycling method to the compressible turbulent ZPGSFPBL. For the most part, the extension is reasonably straightforward in light of the fact that the classical inner and outer scaling on the mean streamwise velocity of the incompressible

ZPGSFPBL can be applied to the Van Driest–transformed compressible streamwise component (Bradshaw 1977). One obvious complicating factor is the treatment of the thermodynamic variables at the inlet. Urbin & Knight (2001) reported LES of an adiabatic ZPGSFPBL at a free-stream Mach number $M_\infty = 3$. In their scheme, the mean wall-normal velocity and all the velocity fluctuations are treated in exactly the same way as in the LWS method. The inlet static pressure is assumed to be constant; the mean temperature and temperature fluctuation are scaled in the same way as used for the mean wall-normal velocity (see also Knight 2006). Urbin & Knight (2001) imposed the empirical correlations from Smits & Dussauge (1996) to estimate the scaling factors,

$$\frac{\delta_{re}}{\delta_{in}} = \left[1 + \left(\frac{x_{re} - x_{in}}{\delta_{in}}\right) 0.27^{\frac{6}{5}} Re_{\delta_{in}}^{-\frac{1}{5}}\right]^{\frac{5}{6}} \quad \text{and} \quad \frac{u_{\tau,in}}{u_{\tau,re}} = \left(\frac{\delta_{re}}{\delta_{in}}\right)^{\frac{1}{10}}. \tag{4}$$

Stolz & Adams (2003) applied a similar procedure in their LES of an isothermal ZPGSFPBL at $M_\infty = 2.5$. Instead of assuming a constant inlet pressure, they chose to perform the same weak recycling procedures on the mean density and density fluctuation as those used on the mean temperature and temperature fluctuation, respectively. Xu & Martin (2004) noted that according to Morkovin's hypothesis (Bradshaw 1977), treatment of the compressibility effects on boundary layer turbulence can be reduced to the consideration of the mean density variation effects. In their scheme, mean wall-normal velocity scaling involves the ratio of the mean local density to the wall density. The temperature fluctuation is linked to the streamwise velocity fluctuation through a generalized functional form analogous to the strong Reynolds analogy (Bradshaw 1977), and the density fluctuation is assumed to be proportional to the temperature fluctuation.

The primary issue in the weak recycling method is the treatment of turbulence fluctuations. Mean velocity statistics for both the compressible and incompressible ZPGSFPBLs are abundant in the forms of experimental and DNS data as well as analytical and empirical correlations, whose accuracy is sufficient for the purpose of inflow turbulence generation. As a matter of fact, Sagaut et al. (2004) reported that when Urbin & Knight's (2001) approach was applied on a ZPGSFPBL at $M_\infty = 2.3$, the averaged statistics, such as the boundary layer thickness δ, exhibited a slow drift in time. Their solution was to fix the mean inflow quantities and perform the weak recycling procedure on the turbulence fluctuations only. This modification was successfully applied by Pirozzoli & Bernardini (2013) in a ZPGSFPBL at $M_\infty = 2$ and up to $Re_\theta = 15,500$. Lagha et al. (2011) adopted a similar approach of fixing the mean inflow quantities in the weak recycling method by prescribing the inflow mean streamwise velocity using a composite profile of Reichardt's inner solution and Finley's wake solution. Their mean inflow temperature profile was prescribed using the Crocco-Busemann approximation. The authors treated the turbulent velocity fluctuations using a procedure analogous to the simplified weak recycling procedure of Spalart et al. (2006) in which the outer scaling is applied throughout the boundary layer without inner scaling, $\mathbf{u}'(x_{in}, y_{in}, z, t + \Delta t) = \mathbf{u}'[x_{re}, (\delta_{re}/\delta_{in})y_{in}, z, t]$. The same approximation was also applied to the temperature and density fluctuations at the inlet. The results of both Lagha et al. (2011) and Pirozzoli & Bernardini (2013) were validated against experimental data and subsequently used for in-depth investigations of the structures and statistics of the compressible ZPGSFPBL.

The spurious periodicity associated with the LWS weak recycling method persists in its compressible variants. This was confirmed by Morgan et al. (2011) in their LES of an adiabatic supersonic ZPGSFPBL at $M_\infty = 2.3$ and $Re_\theta \sim 1,700$ using the approach of Urbin & Knight (2001). The LES domain length is $15\delta_{re}$ and the recycling station is at $x_{re} = 12.7\delta_{re}$. Their spatial-temporal map of the two-point correlation coefficient for the streamwise velocity component $R_{11}(x_{re} + \Delta x, y = 0.7\delta_{re}, z, t + \Delta t)$ exhibits artificial streaks, and in this particular case, it takes a time duration equivalent to approximately $40\,\delta_{re}/U_f$ for these artificial streaks to dissipate. The incorporation of the constant spanwise shift modification of Spalart et al. (2006)

converted an artificial streak in $R_{11}(x_{re} + \Delta x, y = 0.7\delta_{re}, z, t + \Delta t)$ into a new streak in the map of $R_{11}(x_{re}, y = 0.7\delta_{re}, z + \Delta z, t + \Delta t)$. Fortunately, Morgan et al. found that by adjusting the amount of spanwise shift dynamically in a random manner, the spurious periodicity can be substantially weakened. This issue is particularly relevant to computing compressible flows with certain inherent physical low-frequency motion. Inflow generation for such flows using the weak recycling method should incorporate either dynamic shifting or other similar remedies.

Once a high-quality spatially developing supersonic ZPGSFPBL is at hand, one may proceed to eddy simulations on a class of practical aeronautical flow problems characterized by SWBLI. Priebe & Martin (2010) used Xu & Martin's (2004) approach in their DNS of a 24° compression ramp SWBLI with the upstream inflow at $M_\infty = 2.3$ and $Re_\theta = 2,900$. They noted that the coherence between the low-frequency shock-wave motion and the upstream ZPGSFBPL is statistically significant but weak. In a DNS on oblique SWBLI, Pirozzoli & Bernardini (2011) positioned the recycling station relatively far downstream from the inlet at $x_{re} = 42.98\delta_{re}$ in conjunction with a spanwise shift to weaken the strength of the spurious periodicity. Morgan et al. (2014) and Roussel et al. (2015) applied Urbin & Knight's (2001) approach in LES of the SWBLI inside a constant-area duct, which forms a prototype of the supersonic inlet and isolator system. The duct sidewalls prevented them from applying the dynamic reflection procedure of Morgan et al. (2011). The ZPGSFPBL on each wall was first simulated separately followed by summation using the distance-based multiwall weighted averaging procedure developed by Boles et al. (2010).

Another issue in the application of the weak recycling method to the compressible ZPGSFPBL involves the appearance and gradual amplification with time of initially small-amplitude acoustic fluctuations in the free stream. Priebe & Martin (2010) used a filter to damp out such fluctuations outside the typical intermittent zone of the boundary layer. Morgan et al. (2014) used a body force term to create a sponge zone in the core region of their duct near the inlet, which silenced the spurious shock wave and acoustic wave arising from the weak recycling.

2.4. Extension of Weak Recycling to Rough Surface Boundary Layers

The turbulent ZPGRFPBL constitutes a representative model of a wide class of external flows encountered in marine, wind, and aeronautical engineering applications. The flow over turbomachinery blades degraded by the deposition of combustion products or by cavitation is one such example. For eddy simulation of rough surface boundary layers, if the upstream inflow begins with a segment of the ZPGSFPBL, then the LWS weak recycling method can be applied in a straightforward manner, as done in the DNS of Lee & Sung (2007) and Yuan & Piomelli (2015) with a small roughness height to boundary layer thickness ratio k/δ in the range $0.045 \sim 0.125$. These and other studies, such as those reviewed by Jiménez (2004), confirm the existence of a near-wall flow dominated by roughness elements and an outer flow nearly unaware of the roughened surface. The viscous length scale ν/u_τ should be replaced by a more suitable roughness length scale for inner scaling, and evaluation of the friction velocity becomes less straightforward given that the skin friction now includes contributions from both the viscous drag and pressure drag. Thus, when the inlet station is located on a rough surface, modifications on the LWS method are necessary.

For a ZPGRFPBL with small k/δ that can be considered as sand-grain roughened, Nozawa & Tamura (2002) kept the viscous length scale in the LWS method unchanged but incorporated the equivalent sand-grain roughness height k_S into the correlation between θ_{in}/θ_{re} and $u_{\tau,in}/u_{\tau,re}$ with the following sand-grain flat-plate correlation:

$$\frac{\theta_{re}}{\theta_{in}} - 1 = \frac{C_f'}{2}\left(\frac{x_{in}}{\theta_{in}}\right)\frac{1}{1-r}\left[\left(\frac{u_{\tau,in}}{u_{\tau,re}}\right)^{2r-2/r} - 1\right], \quad \text{where} \quad r = \frac{3.95}{2.87 + 1.58\log(x_{in}/k_S)}. \quad (5)$$

Here x_{in} is the distance from the leading edge of the plate to the inlet station estimated based on its correlation with θ_{in}. $C'_f(x_{in})$ is the local skin friction coefficient, and θ_{re}/θ_{in} is computed directly from the simulation. Tamura et al. (2007) used this modification in their LES of flow over hilly terrain with vegetation. Cardillo et al. (2013) also kept the viscous length scale for inner scaling in their DNS of a sandpaper-roughened flat-plate boundary layer with an inlet roughness parameter $k/\delta_{in} \approx 0.014$. The dynamic aspect of their modification on the LWS method involves a test plane inserted approximately midway between the inlet and the recycling station to avoid directly invoking empirical correlations on boundary layer integral parameters. The outer layer scaling is assumed to be unaffected by the surface roughness. The friction velocity ratio $u_{\tau,in}/u_{\tau,re}$ is obtained indirectly through the momentum integral equation $d\theta/dx = (u_\tau/U_f)^2$.

For fully rough boundary layers with large values of k/δ, it is necessary to replace the viscous length scale ν/u_τ in the LWS method with a new penetration length scale l_d characterizing the effect of the roughness elements. Toward this end, Yang & Meneveau (2015) proposed to decompose the velocity as $\mathbf{u}(x, y, z, t) = \langle \tilde{\mathbf{u}} \rangle_z (x, y) + \mathbf{u}''(x, y, z, t)$, so that the deviation $\mathbf{u}''(x, y, z, t)$ with respect to the spanwise averaged mean contains both the turbulence fluctuations and the spanwise inhomogeneity due to the roughness elements. $\tilde{\mathbf{u}}$ is a short-duration, temporally averaged mean obtained from an exponentially weighted procedure. Scaling operations are applied on $\langle \tilde{\mathbf{u}} \rangle_z$ and $\mathbf{u}''$ at the inlet and the recycling stations following the LWS procedure except that the new inner penetration length l_d is used, which is estimated to be the wall distance at which the streamwise dispersive stress component $\langle \tilde{u}\tilde{u} \rangle_z - \langle \tilde{u} \rangle_z^2$ reaches 10% of its local maximum. For the type of fully rough boundary layers considered by Yang & Meneveau (2015), both the friction velocity and the penetration depth are assumed to take the same values between the inlet and recycling station. Another notable advance by Yang & Meneveau (2015) is the modification of the weighting function in the composite velocity profile. As shown in **Figure 1a**, the original blending function $W(y/\delta)$ in the LWS method underestimates the distortion by roughness elements on the streamwise velocity profile. Yang & Meneveau (2015) corrected this with an improved weighting function $W_R(y, \delta, l_d)$.

2.5. Extension of Weak Recycling to Environmental Flows

The weak recycling inflow generation method has been extended to spatially developing LES of many environmental flows, including thermally stratified rough surface boundary layers with pollutant dispersion and microscale urban canopy flow coupled with mesoscale wind predicted from numerical weather prediction (NWP) codes. In many environmental atmospheric flows, the statistical streamwise variation of the boundary layer can often be neglected until a notable downstream change in the surface condition, and the stability associated with thermal stratification has a major impact on turbulence. Another notable feature is that under realistic meteorological conditions, the main wind at the microscale LES domain inlet actually changes with time, and mean flow three-dimensionality due to the Coriolis force may also be a factor.

Mayor et al. (2002) considered the internal boundary layer created by cold air from ashore moving past a large expanse of warm water. The shoreline and their inland recycling station, referred to as the magic slice, are located 4 km and 3 km downstream of the inlet, respectively. At the inlet, the prescribed mean velocity profile was held steady, whereas fluctuations at the magic slice with respect to the locally averaged winds are recycled without rescaling. An analogous approach was adopted by Kataoka (2008), who also reported that a damping function was needed on the recycled fluctuations to prevent excessive free-stream contamination. The region between the inlet and recycling station is often termed the driver region by environmental fluid dynamists. According to Tamura (2008), to generate inflow for a downstream unstably stratified boundary layer inside the driver region, one can apply the approach of Kataoka (2008) on velocity fluctuations, whereas
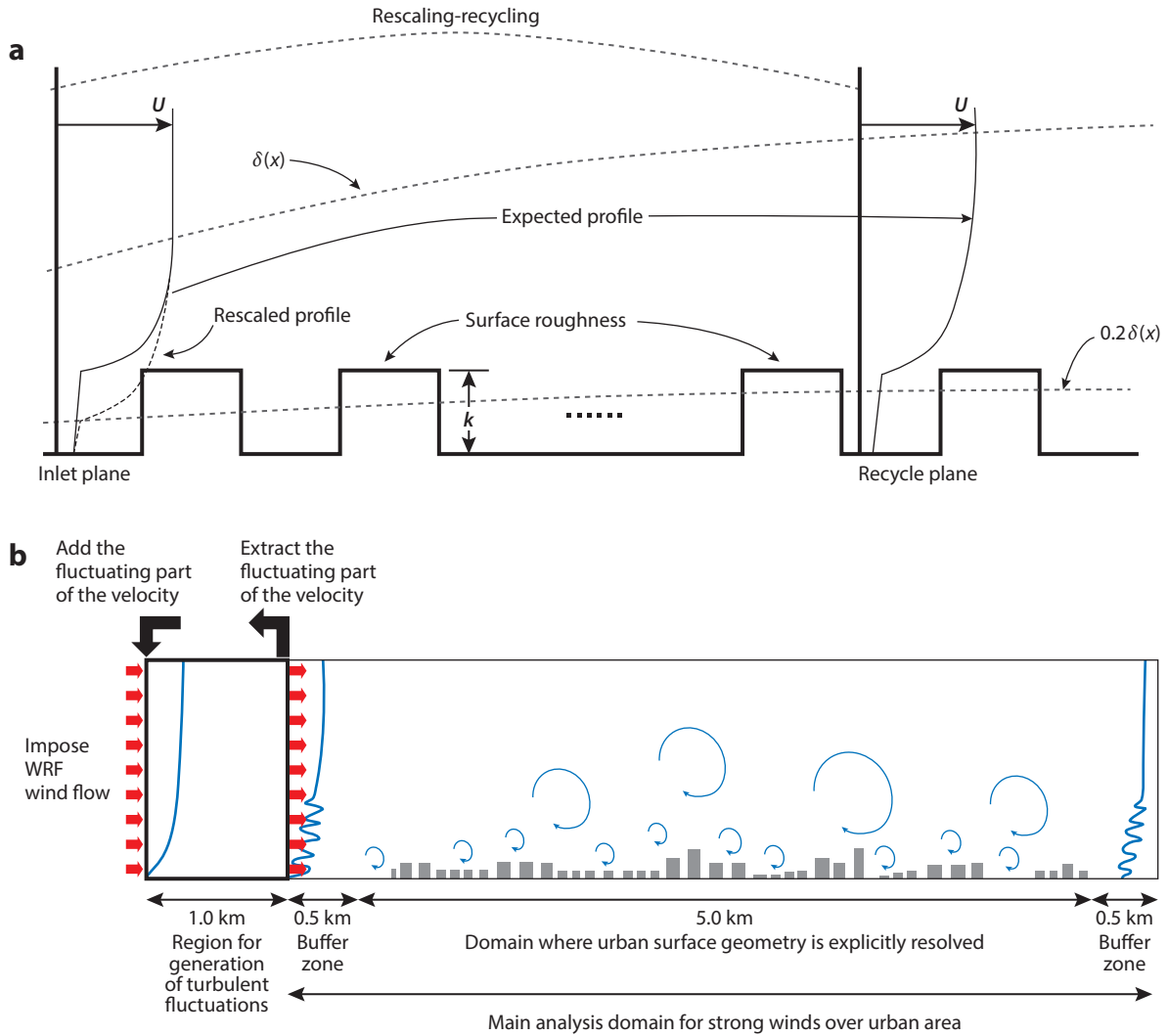
Figure 1

Schematic illustrations of weak recycling inflow turbulence generation for a rough surface boundary layer and urban canopy flow simulations. (*a*) A fully rough boundary layer large-eddy simulation (LES) configuration. The underestimation of the roughness distortion due to the original blending function W of Lund et al. (1998) is corrected with an improved formulation: $W_R = 0$ if $y < l_d$, and $W_R = W [(y - l_d)/(\delta - l_d)]$ if $l_d \leq y < \delta$. Panel *a* adapted with permission from Yang & Meneveau (2015). Copyright Taylor & Francis Ltd. (*b*) Microscale LES configuration for the 2009 event of Typhoon Melor past Tokyo. The transient main wind at the inlet is from a macroscale numerical weather prediction using the Weather Research and Forecasting (WRF) code. Panel *b* reproduced with permission from Nakayama et al. (2012). Copyright John Wiley & Sons, Ltd.

temperature may be treated as a passive scalar. For a stably stratified boundary layer, Tamura (2008) suggested prescribing the mean temperature profile at the inflow boundary of the main simulation domain because the fluctuations of the passive scalar are excessively large for the situation (see also Jiang et al. 2012). In an LES of pollutant dispersion in a thermally stratified complex boundary layer, Tomas et al. (2015) generated the inlet velocity field and temperature field using the approach of Kong et al. (2000) with weak rescaling applied to both the mean and

fluctuations; the damping technique was applied to elevations above 1.2δ. They also fixed the inlet mass flux given that the minor temporal drift in mass flux due to the rescaling procedure and the associated interpolation results in pressure pulses in the domain (Wu & Moin 2009, Wu 2010). Additionally, Tomas et al. (2015) reported that the initialization of their stably stratified boundary layer LES was quite delicate because the flow has a tendency to become relaminarized, and the effect of buoyance had to be introduced gradually into the simulation.

Transient meteorological events such as hurricanes and typhoons can be incorporated into building-resolving urban canopy LES through a nesting and coupling procedure. Mesoscale NWP codes such as the Weather Research and Forecasting computer program simulate the atmospheric flow over a large expanse of area using a set of nested grids. In Nakayama et al.'s (2012) simulation on the 2009 event of Typhoon Melor past Tokyo, the horizontal domain of the microscale LES is inside the smallest nested NWP grid and covers a 6 km × 2 km central district of Tokyo on a horizontal grid spacing of 20 m. The outermost NWP grid covers an area of 1,800 km × 1,900 km with a 4.5-km grid spacing. NWP code outputs can supply the time-varying main winds at the LES inlet as well as the initial condition for the LES, but they are not capable of producing turbulence fluctuations. Nakayama et al. (2012) and Park et al. (2015) applied the approaches of Mayor et al. (2002) and Kataoka (2008) with a hyperbolic tangent damping function to control the excessive fluctuations in the free stream. As shown in **Figure 1b**, in such coupled meteorological simulations, a subsection is often added upstream of the primary urban LES domain to serve as the driver region for the weak recycling. The spurious periodicity issue has so far received little attention in environmental flow simulations.

3. SYNTHETIC INFLOW TURBULENCE GENERATION

3.1. Synthetic Random Fourier Method

Prior to the wide adoption of DNS in fundamental turbulence research, theoreticians often resorted to synthetically constructing pseudo-incompressible HIT for purposes of studying particle dispersion and sound propagation through turbulent media. Kraichnan (1970) developed a divergence-free synthetic HIT approximation through the summation of random Fourier modes, which was subsequently applied by Drummond et al. (1984) and Maxey (1987) in their passive particle and aerosol dispersion studies and by Rogallo (1981) to provide initial conditions for his DNS on the HIT. In Kraichnan (1970), the velocity amplitude corresponding to each wave vector $\mathbf{k}_n$ is not deterministic. When LES started to be applied to CWE in the 1990s, Kraichnan's approximation was quickly recognized as a viable tool for inflow turbulence generation of wind past buildings and other structures (see Kondo et al. 1997, Maruyama et al. 1999, Tamura & Ono 2003, Aboshosha et al. 2015, García et al. 2015, Li et al. 2015). Some of the Japanese CWE researchers attributed the synthetic random Fourier method (SRFM) to work by Hoshiya (1972) on multicorrelated random processes.

For a given energy spectrum $E(k_n)$, the amplitude of the velocity vector associated with wave vector $\mathbf{k}_n$ can be specified deterministically and directly rather than stochastically and indirectly as in Kraichnan (1970) with Gaussian-distributed values corresponding to the specified spectrum. This was achieved by Karweit et al. (1991) and Béchara et al. (1994) in their studies on sound dispersion through a synthetic HIT. The three-dimensional HIT velocity field at one random instant t is approximated as

$$\mathbf{u}_{\text{HIT}}(\mathbf{x}, t) = 2 \sum_{n=1}^{N} \widehat{u}_n(t) \cos(\mathbf{k}_n \cdot \mathbf{x} + \psi_n) \boldsymbol{\sigma}_n, \ \widehat{u}_n(t) = [E(k_n)\Delta k_n]^{1/2} \text{ and } \text{TKE} = \sum_{n=1}^{N} \widehat{u}_n^2 = \int_0^{\infty} E(k)\mathrm{d}k,$$

(6)
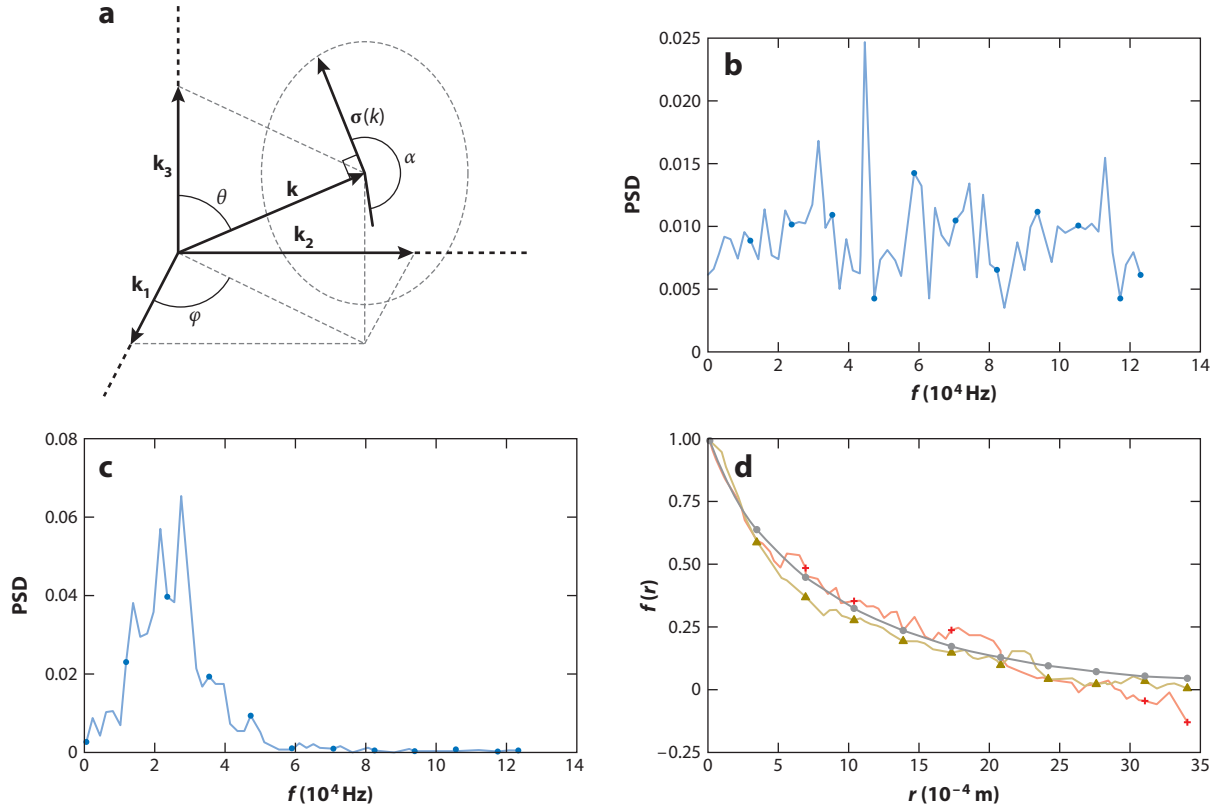
Figure 2

Schematic illustration of the synthetic random Fourier method (SRFM) and effect of the synthetic digital filtering method. (*a*) Definition of a single Fourier wave vector in spherical coordinates. Panel *a* adapted with permission from Karweit et al. (1991). Copyright the Acoustic Society of America. (*b*) Power spectral density (PSD) of an SRFM velocity signal at a given point. The spectrum exhibits typical random number behavior because the SRFM sequence is white noise in time. (*c*) PSD of the same velocity signal after digital filtering through convolution with a Gaussian filter, exhibiting the expected peak frequency and decay. (*d*) Longitudinal two-point correlation function. The circles represent homogeneous isotropic turbulence theory, the triangles are for SRFM before digital filtering, and the plus signs are for SRFM after digital filtering. Panels *b*, *c*, and *d* adapted with permission from Béchara et al. (1994). Copyright the American Institute of Aeronautics and Astronautics.

where ψ_n is the phase associated with $\mathbf{k}_n$, and $\boldsymbol{\sigma}_n$ is a unit direction vector perpendicular to $\mathbf{k}_n$ whose position is determined randomly by its polar angle α_n. The wave vector $\mathbf{k}_n$ is defined by its spherical coordinates (k_n, ϕ_n, θ_n), as shown in **Figure 2a**. Isotropy is achieved by choosing probability density functions (PDFs) for the four random variables as $\mathrm{PDF}(\theta_n) = \sin\theta_n/2$, $\mathrm{PDF}(\phi_n) = 1/(2\pi)$, $\mathrm{PDF}(\alpha_n) = 1/(2\pi)$, and $\mathrm{PDF}(\psi_n) = 1/(2\pi)$, respectively. Béchara et al. (1994) used the Karman-Pao spectrum to simulate the complete spectra. To assign the spectral power to a finite number of N modes, Karweit et al. (1991) considered random, linear, and logarithmic distributions and settled on the logarithmic distribution, which provides a better representation of the velocity characteristics in the lower-wave-number range corresponding to the energy-containing eddies.

Karweit et al. (1991) indirectly specified the spatial correlation through the energy spectrum $E(k_n)$. Béchara et al. (1994) obtained the temporal correlation through digital filtering in the frequency domain. The initial random time series was band-pass filtered using a linear phase

finite impulse response Gaussian filter with a transfer function $\hat{H}(f) = \exp[-(f - f_0)^2/a^2 f_0^2]$ centered on the frequency f_0. The convolution of the raw velocity signal with the inverse Fourier transform of $\hat{H}(f)$ yields a temporally correlated signal exhibiting the power spectral density shown in **Figure 2c**.

Bailly & Juvé (1999) provided another way of introducing time dependence into the synthetic HIT transported by a constant convective velocity vector u_c through modification of the formulation of Béchara et al. (1994),

$$\mathbf{u}_{\text{HIT}}(\mathbf{x}, t) = 2 \sum_{n=1}^{N} \widehat{u}_n(t) \cos\left[\mathbf{k}_n \cdot (\mathbf{x} - t\mathbf{u}_c) + \psi_n + \omega_n t\right] \boldsymbol{\sigma}_n. \tag{7}$$

They also pointed out the need to make the circular frequency ω_n dependent on $\mathbf{k}_n$. The SRFM of Karweit et al. (1991) and Béchara et al. (1994) has been applied to inflow turbulence generation for CAA and other applications (see Billson et al. 2004, Gloerfelt & Garrec 2008, Tabor & Baba-Ahmadi 2010). Even though the velocity field so constructed has an unphysical zero skewness factor, the SRFM distinguishes itself from other synthetic methods with its lack of ad hoc adjustable parameters.

According to Le & Moin (1994), an anisotropic turbulent flow $\mathbf{u}(\mathbf{x})$ with known Reynolds stress tensor $\mathbf{R}$ and mean flow field $\langle \mathbf{u} \rangle (\mathbf{x})$ may be approximated as $\mathbf{u}(\mathbf{x}, t) = \langle \mathbf{u} \rangle (\mathbf{x}) + \mathbf{A}\mathbf{u}_{\text{HIT}}(\mathbf{x}, t)$, where tensor $\mathbf{A}$ is the Cholesky decomposition of $\mathbf{R}$, and its components are given in the appendix of Lund et al. (1998). As a result of the above transformation, the anisotropic field $\mathbf{u}(\mathbf{x}, t)$ may not satisfy the continuity equation and the spatial correlations initially imposed on the synthetic $\mathbf{u}_{\text{HIT}}(\mathbf{x}, t)$. Remedy SRFM schemes considering both the divergence-free constraint and spatial inhomogeneity and anisotropy were reported by Smirnov et al. (2001), Huang et al. (2010), Castro & Paz (2013), and Yu & Bai (2014), which often involve the introduction of new ad hoc parameters and assumptions. Nonuniform mesh can be easily accommodated by first performing the SRFM procedures on an auxiliary uniform mesh, followed by subsequent interpolation. A comparative study between SRFM and weak recycling in a CWE application (LES of wind past tall buildings) was reported by Yan & Li (2015). It was found that grid resolution inside the driver region is important in the performance of the weak recycling method, and the SRFM can yield satisfactory results in a CWE application provided that a realistic energy spectrum is specified for the atmospheric boundary layer.

3.2. Synthetic Digital Filtering Method

In Béchara et al. (1994), the SRFM-generated pseudo-HIT field at any single instant is spatially correlated through the imposed energy spectrum (**Figure 2d**), but the fields at different instants are nevertheless without any temporal correlation and may be viewed as white noise in time (**Figure 2b**). Temporal coherence was imposed by Béchara et al. through digital filtering of the random temporal sequence through convolution with a Gaussian filter (**Figure 2c**). The same idea can of course be extended to imposing spatial coherence on data points that are initially random in space for the purpose of synthetic inflow turbulence generation. This was pursued by Klein et al. (2003).

To construct a one-dimensional array of data u_m that are equally spaced in x with a prescribed two-point correlation coefficient $R_{uu}(j\Delta x)$, one may start with a longer one-dimensional sequence of random data points r_m with $\langle r_m \rangle = 0$ and $\langle r_m r_i \rangle = \delta_{mi}$, together with a digital, linear, nonrecursive filter with support extent N and filter coefficients b_i. Convolution in the physical space yields $u_m = \sum_{i=-N}^{N} b_i r_{m+i}$. The filter coefficients b_i can in principle be determined based on any known types of correlation function (di Mare et al. 2006), but in practice explicit approximate solutions

can be obtained only in a few special cases, such as the exponential or Gaussian correlation function. By assuming an exponential correlation $R_{uu}(j\Delta x) = \exp\left[-\pi\,|j|\,/(2M)\right]$ with a length scale $M\Delta x$, Xie & Castro (2008) obtained the filter coefficients as

$$b_j = \tilde{b}_j / \sqrt{\sum_{i=-N}^{N} \tilde{b}_i^2}, \text{ where } \tilde{b}_j \approx \exp\left(-\frac{\pi\,|j|}{M}\right). \tag{8}$$

Temporal correlation was assumed to obey an exponentially decaying form with a characteristic timescale T,

$$u_m(t + \Delta t) = u_m(t)\exp\left(-\frac{\pi\Delta t}{2T}\right) + u_{m\beta}(t)\left[1 - \exp\left(-\frac{\pi\Delta t}{T}\right)\right]^{0.5}, \tag{9}$$

where $u_{m\beta}$ is calculated in the same manner as u_m but using an independent set of random data r_m. Extension of the above synthetic digital filtering method (SDFM) to multidimensions is straightforward (Klein et al. 2003, Xie & Castro 2008), but at a significantly increased computational cost. Optimization of the multidimensional implementation of the SDFM as well as introduction of spatially varying integral length scales including cross-integral length scales was discussed by Veloudis et al. (2007), Fathali et al. (2008), and Kempf et al. (2012). The divergence-free constraint is rarely imposed in the SDFM, but one plausible implementation was proposed by Kim et al. (2013). From an engineering point of view, the attractive feature of the SDFM is its ability to impose a two-point spatial correlation directly rather than indirectly through an energy spectrum as in the SRFM.

It is customary to demonstrate the effectiveness of synthetic turbulence generation methods by feeding the manufactured solution into a complex spatially developing simulation. Actually, one convincing measure for checking the quality and fidelity of the constructed pseudo-HIT is to compare its temporal decay characteristics with benchmark data. Dietzel et al. (2014) performed a careful comparative study on the temporal decay of three-dimensional pseudo-HIT fields manufactured using the SRFM and SDFM. Their results show that the decay characteristics of the HIT, as measured by an energy spectrum as well as longitudinal and transverse velocity correlations, are well captured by the initial velocity field constructed using the SRFM. The results from the SDFM at the same time display relatively large discrepancies compared to experimental data, most likely because only one integral length scale is supplied as input as opposed to the entire energy spectrum together with the overly simplified exponential or Gaussian correlation function. Pseudoturbulence generated using the SDFM has been applied as an inflow condition for combustion LES by Saghafian et al. (2015), among others. Applications of the SDFM to SWBLI and CAA simulations were reported by Touber & Sandham (2009) and Dhamankar et al. (2015), respectively.

3.3. Synthetic Coherent Eddy Method

The SRFM and SDFM attempt to model inflow turbulent eddying motion indirectly from a statistical point of view by imposing constraints on random number fields through an energy spectrum or correlation function to account for the eddies' spatial and temporal coherence. An alternative view is that it may be more physically sound, at least for wall-bounded anisotropic flows, to directly mimic the representative coherent eddies of turbulent flow from a structural point of view. This is the basic idea of the synthetic coherent eddy method (SCEM). The mathematical procedures entailed in SCEM have been demonstrated by Jarrin et al. (2006) using a one-dimensional flow example (see also Kornev & Hassel 2007). Essentially, the flow is assumed to consist of randomly distributed turbulent spots, which are characterized by shape function f_σ with compact support

and satisfying a proper normalization condition. The spots are assumed to be convected downstream with a constant reference velocity using Taylor's frozen turbulence hypothesis. Proper choice of the shape function is an important element in the SCEM method. The shape function used in Jarrin et al. (2006) is Gaussian, which allows easy satisfaction of a prescribed two-point correlation function, but other more complex functions may also be applied at the expense of introducing more empirical adjustable parameters. The SCEM of Sandham et al. (2003) and Li & Coleman (2004) splits a boundary layer into an inner region modeled with lifted streaks and an outer region populated with three-dimensional vortices. Pamiès et al. (2009) extended the SCEM to the ZPGSFPBL by slitting the inlet plane into multiple zones, such as the logarithmic zone and wake zone, each with its distinct shape function characterizing the locally representative coherent structures. Enforcement of the divergence-free constraint in the SCEM was discussed by Poletto et al. (2013).

The philosophy embedded in the SCEM can be traced back to Perry & Chong (1982) and Marusic & Perry (1995), who suggested that mean and second-order statistics of the ZPGSFPBL could be reproduced to a satisfactory degree through direct superposition of the representative coherent eddy structures. Following this line of thought, Subbareddy et al. (2006) proposed a variant of the SCEM for inflow turbulence generation of the compressible ZPGSFPBL. The flow was assumed to be populated by simplified hairpin vortex skeletons consisting of straight-line segments attached to the wall (**Figure 3a**). Image vortices were used to guarantee zero normal velocity at the wall, and a Van Driest type of damping function was applied to enforce the no-slip boundary condition. The Biot-Savart law was used to compute the velocity field arising from the randomly distributed eddies at each grid point. Recent DNS results of the fully turbulent ZPGSFPBL developed from an upstream bypass transition in the narrow sense (Wu et al. 2014) provide accurate and unequivocally clear evidence that the representative coherent structure in the near-wall region (beneath the lower logarithmic layer) is turbulent-turbulent spot packed with small-scale hairpin vortices, whereas that in the outer wake region is a densely packed grove of large-scale hairpin vortices (see **Figure 3b,c**). Although slightly less distinct given their existence in a chaotic turbulent environment, these turbulent-turbulent spots nevertheless bear certain similarities to the commonly known transitional turbulent spots, which are also packed with hairpin vortices. The smallest size of the hairpin vortices forming the turbulent-turbulent spots observed is approximately 20 wall units in width. This evidence offers general philosophical support to the underlying assumption used by Marusic & Perry (1995) and Subbareddy et al. (2006), and also to the random turbulent spot assumption of Jarrin et al. (2006). LES applications of the SCEM in jet flow and CAA studies were reported by Abboud & Smith (2014) and Kim & Haeri (2015), respectively.

3.4. Synthetic Volume Forcing Method

Properly designed synthetic body force terms added to the Navier-Stokes equation system within a control zone can accelerate the development process into turbulence starting from either an upstream laminar velocity profile or a synthetically constructed pseudoturbulent profile. Such body force terms should be strong enough to produce rapid transition but at the same time be sufficiently weak to avoid leaving notable footprints in the downstream turbulent region.

Spille-Kohoff & Kaltenbach (2001) applied a wall-normal dynamic forcing in their LES of the ZPGSFPBPL with the same type of inflow condition as in Le et al. (1997), namely turbulent mean and second-order statistics from Spalart (1988) and fluctuations from the SRFM of Lee et al. (1992) rescaled using the Cholesky decomposition. The body force was applied within a control zone adjacent to the inlet, and its magnitude was adjusted dynamically to minimize the difference

Figure 3

Schematic illustration and direct numerical simulation evidence for the underlying random turbulent spot assumption used in the synthetic coherent eddy method. (*a*) Eddy box formed by modeled hairpin vortices. Panel *a* adapted with permission from Subbareddy et al. (2006). Copyright P. Subbareddy. (*b*) Turbulent-turbulent spots formed by small-scale hairpin vortices beneath the lower logarithmic region in a zero-pressure-gradient smooth flat-plate boundary layer (ZPGSFPBL) at $Re_\theta \sim 2,700$. Blue and red correspond to $y^+ = 0$ and 120, respectively. (*c*) Dense groves of hairpin vortices in the wake region of a ZPGSFPBL at $Re_\theta \sim 2,700$. Blue and red correspond to $y/\delta = 0.6$ and 1.0, respectively. The valley between the groves corresponds to the deep penetration of the free stream into the wall region.
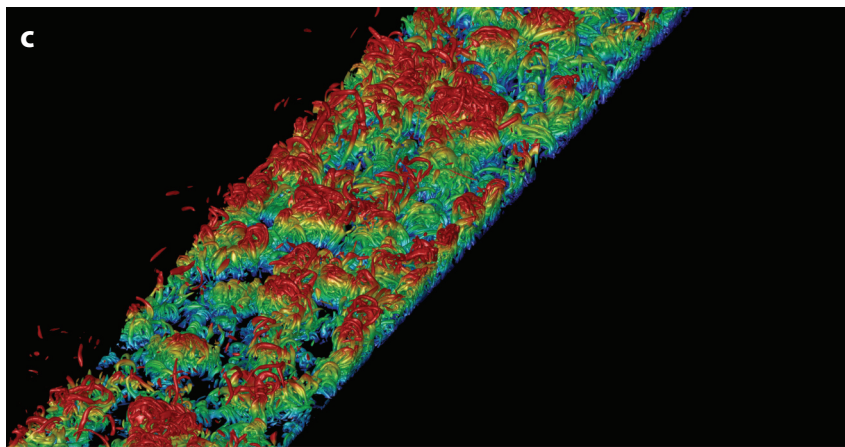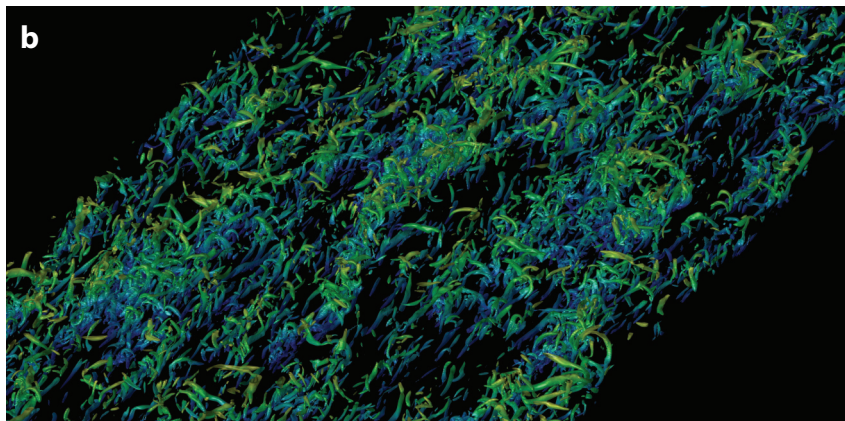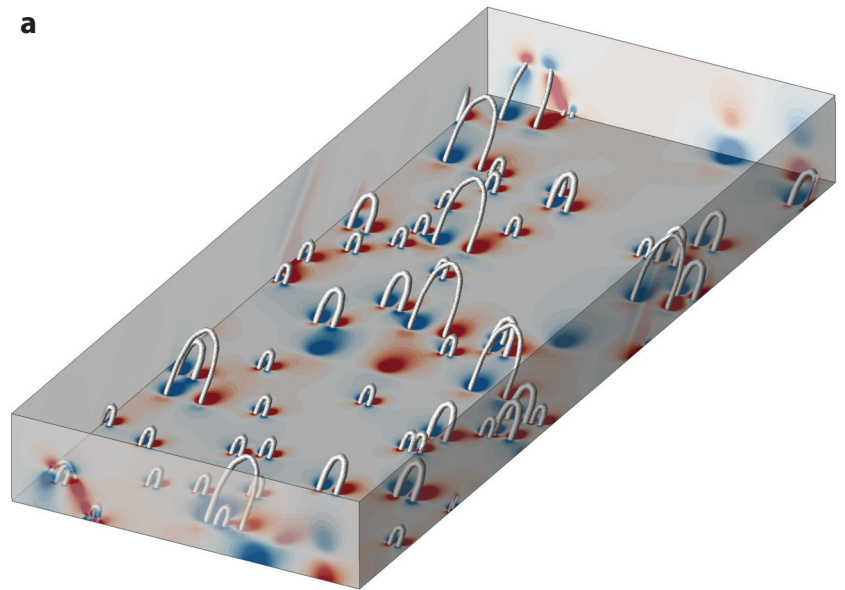
between the computed and targeted Reynolds shear stress profiles. Keating et al. (2004) tested this approach in channel flow and found that it yielded superior performance compared to the weak recycling method and the SRFM. They also noted that an important element in facilitating rapid development into turbulence from a synthetic profile is resolving large eddies with dimensions on the order of the integral length scale of the flow.

Schlatter & Örlü (2010, 2012) and Khujadze & Oberlack (2004) applied random volume forcing in the wall-normal direction in DNS to promote an upstream Blasius velocity profile to transition into a fully turbulent incompressible ZPGSFPBL. A control zone with synthetic forcing is defined using spatial Gaussian attenuation. The actual forcing function accommodates specified temporal and spanwise frequencies. A related traditional approach directly applied to the wall-normal velocity component is the use of a synthetic disturbance strip (degenerated volume) along the spanwise direction at the wall to speed up transition through numerical blowing and suction (see Sayadi et al. 2013, and references therein). An analogous controlled synthetic blowing and suction technique was applied by Pirozzoli et al. (2004) and Franko & Lele (2014) to accelerate the supersonic boundary layer transition with and without pressure gradients, respectively. Mullenix et al. (2013) noted that the aforementioned synthetic volume forcing methods (SVFMs) prescribe distinct frequencies and length scales, which may persist into the downstream fully turbulent region of interest. They introduced a simulated plasma-induced electric body force term inside the control section of a supersonic ZPGSFPBL to create an artificial separation bubble, which induced rapid transition without generating strong shock waves. It should be cautioned that the length scale of the separation bubble might still be propagated downstream, and any potential wandering of the separation bubble could also induce unintended spurious frequency. Synthetic volume forcing can also be applied to more complex flows. Pierce & Moin (1998) used an azimuthal body force term to create an axially homogeneous swirling inlet condition for their LES of turbulent flow through a coaxial jet combustor.

In stratified atmospheric flow simulations, the issue of generating inflow turbulence for microscale LES coupled with mesoscale NWP code can be tackled using approaches other than the weak recycling method. Mirocha et al. (2014) and Muñoz-Esparza et al. (2015) applied targeted random potential temperature perturbation in a control zone at selected vertical locations to break the two-dimensionality of the mesoscale flow. Muñoz-Esparza et al. compared the effect of this forcing method with that of the SDFM of Xie & Castro (2008) on a neutral rough boundary layer under the effect of Coriolis force. They reported that transition to turbulence was significantly accelerated with the potential temperature perturbation volume forcing.

3.5. Other Synthetic Methods

Experimentalists have also recognized the importance of accurate inflow turbulence generation for LES and DNS and proposed making use of time-dependent turbulent signals collected from hot-wire probes and particle image velocimetry (PIV) to reconstruct the inlet turbulent flow field (see Druault et al. 2004, Maruyama et al. 2012). Because hot-wire data are limited by the finite number of probe locations, and PIV data often suffer from low temporal resolution (Wallace & Vukoslavčević 2010), advanced reconstruction techniques such as linear stochastic estimation and proper orthogonal decomposition are therefore necessary. Limited success following this approach has been reported on plane mixing layer and channel flow by Perret et al. (2006, 2008) and Johansson & Andersson (2004). With recent advances in time-resolving PIV (Westerweel et al. 2013), it is likely that future experimental data with concurrent high temporal and spatial resolution can be directly applied to inflow turbulence generation with minimal reconstruction, at least for free-shear flows.

Kempf et al. (2005) noted that proper diffusion of a white noise field is equivalent to convolving the field with a Gaussian filter. This allowed them to devise an inflow generator that mimics the effect of the SDFM. Their method imposes spatial coherence on an initially random data field through the solution of an unsteady diffusion equation over a certain time duration to achieve the desired length scale. The method is more suitable for complex geometry and unstructured grids than the original SDFM, but at the expense of adding a differential equation solver. Dietzel et al. (2014) also evaluated the performance of this method in their comparative study using HIT.

4. APPLICATIONS IN HYBRID REYNOLDS-AVERAGED NAVIER-STOKES AND LARGE-EDDY SIMULATION

Zonal wall-modeled hybrid RANS-LES is being adopted as an engineering tool in aerodynamic and CAA applications. The presence of an upstream LES inlet or a downstream RANS-to-LES interface in these hybrid settings has attracted nearly all the aforementioned inflow generation methods into this realm. In the SWBLI calculation of Xiao et al. (2003) and Fan et al. (2004), the upstream supersonic ZPGSFPBL was resolved by LES in the outer layer and by RANS in the near-wall region with an intermediate blending zone in between. The inflow condition for LES was generated following the compressible weak recycling approach of Urbin & Knight (2001). To prevent drifting of the solutions with time (Sagaut et al. 2004), Xiao et al. fixed the inflow mean velocity and temperature profiles. Inflow turbulence model variables can be acquired by applying a similar set of assumed scaling approximations. For example, Xiao et al. scaled turbulent kinetic energy in the same manner as the temperature fluctuation.

It is sometimes useful to superimpose, at the RANS-to-LES inlet, spatially and temporally correlated fluctuations onto the local RANS solution to avoid relaminarization of the LES component (Batten et al. 2004) (see also **Figure 4**). This is particularly necessary when the flow treated by the LES lacks a tangential instability mechanism to excite the Kelvin-Helmholtz instability,
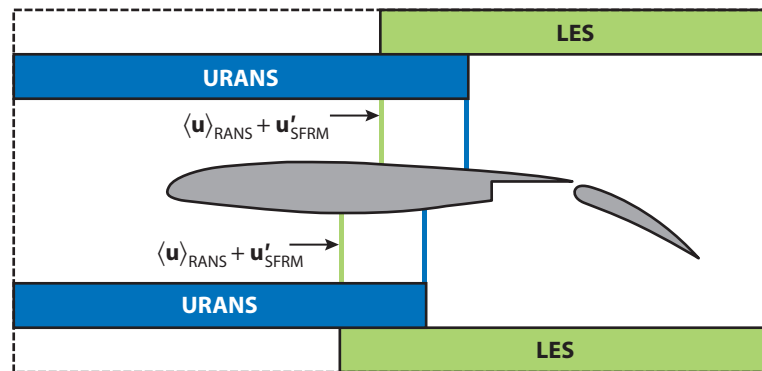
Figure 4

Schematic illustration of the zonal hybrid RANS-LES on a wing-flap configuration. The turbulent inflow at the RANS-to-LES interface is generated using the SRFM of Béchara et al. (1994) superimposed on the RANS solution with an additional internal damping layer inside the overlapping zone to suppress the pressure pulses near the interface. Abbreviations: LES, large-eddy simulation; RANS, Reynolds-averaged Navier-Stokes; SRFM, synthetic random Fourier method; URANS, unsteady Reynolds-averaged Navier-Stokes. Figure adapted with permission from Shur et al. (2014). Copyright Springer.

which is absolutely unstable for all wavelengths. Of course, the weak recycling method could be an option if the local flow is a ZPGSFPBL or the like. But in general it may be more efficient to invoke a suitable synthetic method to generate fluctuations to be superimposed onto the RANS solution. In their hybrid simulation on the channel flow, Batten et al. (2004) applied a simplified version of the Kraichnan SRFM to generate pseudo-HIT followed by tensor scaling to account for anisotropy (Lund et al. 1998). Davidson & Billson (2006) used a similar technique in a channel flow calculation to impose pseudo-turbulent fluctuations at the LES and RANS interface parallel to the wall. They employed the SRFM of Béchara et al. (1994) and presented a useful detailed account of the implementation. However, it is unclear if the imposition of pseudoturbulent fluctuations at such wall-parallel RANS-LES interface is necessary.

Keating et al. (2006) and De Prisco et al. (2008) applied the SVFM of Spille-Kohoff & Kaltenbach (2001) to generate inflow turbulence for the LES inlet in their hybrid calculations of a flat-plate boundary layer under favorable, zero, and adverse pressure gradients. Their setting is analogous to that in **Figure 4**, and the RANS solution within the overlapping region is used to supply statistics and controlled forcing for the generation and development of synthetic turbulence in the LES region. They found that a proper running average scheme is crucial for the success of the method given that it relies on the feedback control of the sampled Reynolds stress toward the target Reynolds stress. A more generalized formalization of the SVFM in zonal hybrid RANS-LES was presented by De Laage de Meux et al. (2015).

Garnier (2009) and Deck et al. (2011) used the SCEM of Jarrin et al. (2006) and Pamiès et al. (2009) in hybrid simulations of SWBLI and an incompressible ZPGSFPBL, respectively. Roidl et al. (2013) modified the SCEM of Pamiès et al. (2009) by using a set of more realistic eddy length scales away from the wall and applied the approach to a hybrid simulation on both the incompressible and supersonic ZPGSFPBLs in which an upstream RANS is followed by a downstream LES with an overlap zone. Laraufie et al. (2011) combined the SCEM of Pamiès et al. (2009) and the SVFM of Spille-Kohoff & Kaltenbach (2001) in their hybrid RANS-LES on the ZPGSFBPL up to $Re_\theta = 31,000$. Their simulation setup is analogous to that in Roidl et al. (2013) except for the addition of a control zone for application of the dynamic forcing, and the modeling of the near-wall region of the downstream LES with RANS. Instead of using a target Reynolds shear stress as the controller for the forcing, Laraufie et al. (2011) found that the wall-normal Reynolds stress component provided a better parameter for the dynamic controlling process. Schmidt & Breuer (2015) integrated the SDFM of Klein et al. (2003) and Xie & Castro (2008) into their hybrid RANS-LES of channel flow and a complex boundary layer.

Inflow turbulence generation is also an important issue for jet engine CFD (Tyacke & Tucker 2015). Schlüter et al. (2004, 2005) developed an approach for integrated RANS-LES-RANS computation of flow through a full jet engine in which the combustor section was simulated using LES, whereas both the compressor and turbine sections were computed using unsteady RANS. The inflow condition to the LES was constructed with the aid of an auxiliary database for turbulence fluctuations scaled by the RANS solution.

Shur et al. (2014) presented an insightful study on inflow turbulence generation in zonal wall-modeled hybrid RANS-LES for aeroacoustics prediction (see **Figure 4**). Pseudo-HIT fields were generated using a slightly modified version of the SRFM of Karweit et al. (1991) and Béchara et al. (1994). In Shur et al.'s implementation of the SRFM, the set of wave numbers is fixed in time and over the entire RANS-to-LES interface, forming a geometrical series distribution. Furthermore, all the random quantities entering Equation 6 were generated only once at the beginning of the simulation so that there are no random changes in phase. To suppress the spurious noise created by synthetic turbulence at the RANS-to-LES interface, Shur et al. (2014) proposed inserting

an internal damping layer placed within the overlapping region. Inside this layer at each time step, a modified LES pressure field is constructed by weighting the RANS pressure and LES pressure from the previous time step. The velocity and temperature fields within the layer remain unmodified, and the density is recomputed with the use of the modified pressure to match the equation of state. Shur et al. (2014) demonstrated a positive effect of the internal damping layer in their CAA calculations of turbulent flows past a trailing edge and over a two-element wing-flap airfoil configuration.

FUTURE ISSUES

1. The interaction between inflow turbulence generation methods and nonreflecting compressible inlet boundary condition schemes (Freund 1997, Colonius 2004) needs to be studied to minimize inflow acoustic disturbance and spurious shock-wave production. A notable exploration in this direction was initiated by Gloerfelt & Garrec (2008).

2. We need to develop more accurate weak recycling and synthetic methods tailored for both compressible and incompressible rough inlet boundary layers. The potential effect of the spurious periodicity of weak recycling in rough surface boundary layers and in environmental atmospheric flow simulations should also be investigated.

3. Synthetic methods for compressible HIT with high turbulent Mach numbers and/or a high ratio of dilatational to solenoidal kinetic energy should be developed. There is also a need to develop and calibrate inflow turbulence generation methods for hypersonic hybrid RANS-LES.

4. More comprehensive calibration studies should be performed on existing synthetic generation methods using both temporally and spatially decaying HIT, following the temporal study of Dietzel et al. (2014).

5. It will be useful for the purpose of simulating environmental flows to develop more consistent and robust weak recycling procedures, synthetic methods, and associated initialization steps for stably and unstably stratified complex boundary layers with mean flow three-dimensionality.

6. We need to study the potential impact of boundary layer temporal and spanwise length-scale disparity when the weak recycling station is positioned very far downstream from the inlet. The implementations of the weak recycling method and synthetic methods in the presence of multiple walls should be improved and calibrated. It would be useful to study the cause of, and develop consistent remedies for, free-stream spurious disturbances in the weak recycling method and synthetic methods. There is also a need to investigate the distance it takes for a canonical compressible/incompressible flat-plate boundary layer to forget its weak recycling/synthetic inflow turbulence.

7. The robustness of synthetic methods should be improved at the RANS-to-LES interface, together with a reduction of the associated ad hoc input parameters and standardization of the various adjustment zone lengths. The pressure pulse and noise generation need to be minimized at such interfaces for CAA problems.

8. Different versions of the SCEM should be integrated, and the shape function set and input parameter set should be standardized. The residual footprints of the imposed control body-force terms in the downstream turbulent region of the SVFM need to be evaluated.

9. Follow-up studies would be welcome to confirm and further explain the spontaneous generation (without relying on downstream convection) of spurious periodicity in the strong recycling method identified by Nikitin (2007).

10. Weak recycling and synthetic methods need to be tailored for renewable energy applications, such as wind turbine farm and tidal turbine flows. Notable recent efforts in this direction have been reported by Gopalan et al. (2014), Keck et al. (2014), Rai et al. (2016), and Munters et al. (2016) (see also Stevens & Meneveau 2017 in this volume).

DISCLOSURE STATEMENT

The author is not aware of any biases that might be perceived as affecting the objectivity of this review.

ACKNOWLEDGMENTS

LITERATURE CITED

Abboud AW, Smith ST. 2014. Large eddy simulation of a coaxial jet with a synthetic turbulent inlet. *Int. J. Heat Fluid Flow* 50:240–53

Aboshosha H, Elshaer A, Bitsuamlak GT, El Damatty A. 2015. Consistent inflow turbulence generator for LES evaluation of wind-induced responses for tall buildings. *J. Wind Eng. Ind. Aerodyn.* 142:198–216

Araya G, Castillo L, Hussain F. 2015. The log behaviour of the Reynolds shear stress in accelerating turbulent boundary layers. *J. Fluid Mech.* 775:189–200

Araya G, Castillo L, Meneveau C, Jansen K. 2011. A dynamic multi-scale approach for turbulent inflow boundary conditions in spatially developing flows. *J. Fluid Mech.* 670:581–605

Araya G, Jansen K, Castillo L. 2009. Inlet condition generation for spatially developing turbulent boundary layers via multiscale similarity. *J. Turbul.* 10:N36

Arolla SK, Durbin PA. 2014. *Generating inflow turbulence for eddy simulation of turbomachinery flows*. Presented at AIAA Aerosp. Sci. Meet., 52nd, National Harbor, MD, AIAA Pap. 2014-0593

Bailly C, Juvé D. 1999. *A stochastic approach to compute subsonic noise using linearized Euler's equations*. Presented at AIAA/CEAS Aeroacoust. Conf. Exhib., 5th, AIAA Pap. 1999-1872

Batten P, Goldberg U, Chakravarthy S. 2004. Interfacing statistical turbulence closures with large-eddy simulation. *AIAA J.* 42:485–92

Béchara W, Bailly C, Lafon P, Candel SM. 1994. Stochastic approach to noise modeling for free turbulent flows. *AIAA J.* 32:455–63

Billson M, Eriksson LE, Davidson L. 2004. *Jet noise modeling using synthetic anisotropic turbulence*. Presented at AIAA/CEAS Aeroacoust. Conf., 10th, Manchester, UK, AIAA Pap. 2004-3028

Boles JA, Choi JI, Edwards JR, Baurle RA. 2010. *Multi-wall recycling rescaling method for inflow turbulence generation*. Presented at AIAA Aerosp. Sci. Meet., 48th, Orlando, FL, AIAA Pap. 2010-1099

Bradshaw P. 1977. Compressible turbulent shear layers. *Annu. Rev. Fluid Mech.* 9:33–54

Cardillo J, Chen Y, Araya G, Newman J, Jansen K, Castillo L. 2013. DNS of a turbulent boundary layer with surface roughness. *J. Fluid Mech.* 729:603–37

Castro HG, Paz RR. 2013. A time and space correlated turbulence synthesis method for Large Eddy Simulations. *J. Comput. Phys.* 235:742–63

Chung YM, Sung HJ. 1997. Comparative study of inflow conditions for spatially evolving simulation. *AIAA J.* 35:269–74

Colonius T. 2004. Modeling artificial boundary conditions for compressible flow. *Annu. Rev. Fluid Mech.* 36:315–45

Davidson L, Billson M. 2006. Hybrid LES-RANS using synthesized turbulent fluctuations for forcing in the interface region. *Int. J. Heat Fluid Flow* 27:1028–42

De Laage de Meux B, Audebert B, Manceau R, Perrin R. 2015. Anisotropic linear forcing for synthetic turbulence generation in large eddy simulation and hybrid RANS/LES modeling. *Phys. Fluids* 27:035115

De Prisco G, Piomelli U, Keating A. 2008. Improved turbulence generation technique for hybrid RANS/LES calculations. *J. Turbul.* 9:N5

Deck S, Weiss PÉ, Pamiès M, Garnier E. 2011. Zonal detached eddy simulation of a spatially developing flat plate boundary layer. *Comput. Fluids* 48:1–15

Dhamankar NS, Blaisdell GA, Lyrintzis AS. 2015. *An overview of turbulent inflow boundary conditions for large eddy simulations*. Presented at AIAA Comput. Fluid Dyn. Conf., 22nd, Dallas, TX, AIAA Pap. 2015-3213

di Mare L, Klein M, Jones WP, Janicka J. 2006. Synthetic turbulence inflow conditions for large-eddy simulation. *Phys. Fluids* 18:025107

Dietzel D, Messig D, Piscaglia F, Montorfano A, Olenik G, et al. 2014. Evaluation of scale resolving turbulence generation methods for large eddy simulation of turbulent flows. *Comput. Fluids* 93:116–28

Druault P, Lardeau S, Bonnet JP, Coiffet F, Delville J, et al. 2004. Generation of three-dimensional turbulent inlet conditions for large-eddy simulation. *AIAA J.* 42:447–56

Drummond IT, Duane S, Horgan RR. 1984. Scalar diffusion in simulated helical turbulence with molecular diffusivity. *J. Fluid Mech.* 138:75–91

Fan CC, Xiao X, Edwards JR, Hassan HA, Baurle RA. 2004. Hybrid large-eddy/Reynolds-averaged Navier-Stokes simulations of shock-separated flows. *AIAA J. Spacecr. Rockets* 41:897–906

Fathali M, Klein M, Broeckhoven T, Lacor C, Baelmans M. 2008. Generation of turbulent inflow and initial conditions based on multi-correlated random fields. *Int. J. Numer. Methods Fluids* 57:93–117

Ferrante A, Elghobashi SE. 2004. A robust method for generating inflow conditions for direct simulations of spatially-developing turbulent boundary layers. *J. Comput. Phys.* 198:372–87

Franko KJ, Lele S. 2014. Effect of adverse pressure gradient on high speed boundary layer transition. *Phys. Fluids* 26:024106

Freund JB. 1997. Proposed inflow/outflow boundary conditions for direct computation of aerodynamic sound. *AIAA J.* 35:740–42

García J, Muñoz-Paniagua J, Jiménez A, Migoya E, Crespo A. 2015. Numerical study of the influence of synthetic turbulent inflow conditions on the aerodynamics of a train. *J. Fluids Struct.* 56:134–51

Garnier E. 2009. Stimulated detached eddy simulation of three-dimensional shock/boundary layer interaction. *Shock Waves* 19:479–86

Gloerfelt X, Le Garrec T. 2008. *Generation of inflow turbulence for aeroacoustic applications*. Presented at AIAA/CEAS Aeroacoust. Conf., 14th, Vancouver, AIAA Pap. 2008-2926

Gopalan H, Gundling C, Brown K, Roget B, Sitaraman J, et al. 2014. A coupled mesoscale-microscale framework for wind resource estimation and farm aerodynamics. *J. Wind Eng. Ind. Aerodyn.* 132:13–26

Hoshiya M. 1972. Simulation of multi-correlated random process and application to structural vibration problems. *Proc. JSCE* 204:121–28

Huang SH, Li QS, Wu JR. 2010. A general inflow turbulence generator for large eddy simulation. *J. Wind Eng. Ind. Aerodyn.* 98:600–17

Jarrin N, Benhamadouche S, Laurence D, Prosser R. 2006. A synthetic-eddy-method for generating inflow conditions for large-eddy simulations. *Int. J. Heat Fluid Flow* 27:585–93

Jewkes JW, Chung YM, Carpenter PW. 2011. Modification to a turbulent inflow generation method for boundary layer flows. *AIAA J.* 49:247–50

Jiang G, Yoshie R, Shirasawa T, Jin X. 2012. Inflow turbulence generation for large eddy simulation in non-isothermal boundary layers. *J. Wind Eng. Ind. Aerodyn.* 104–6:369–78

Jiménez J. 2004. Turbulent flows over rough walls. *Annu. Rev. Fluid Mech.* 36:173–96

Jiménez J, Hoyas S, Simens MP, Mizuno Y. 2010. Turbulent boundary layers and channels at moderate Reynolds numbers. *J. Fluid Mech.* 657:335–60

Johansson PS, Andersson HI. 2004. Generation of inflow data for inhomogeneous turbulence. *Theor. Comput. Fluid Dyn.* 18:371–89

Kalitzin G, Wu X, Durbin PA. 2003. DNS of fully turbulent flow in a LPT passage. *Int. J. Heat Fluid Flow* 24:636–44

Karweit M, Blanc-Benon Ph, Juvé D, Comte-Bellot G. 1991. Simulation of the propagation of an acoustic wave through a turbulent velocity field: a study of phase variance. *J. Acoust. Soc. Am.* 89:52–62

Kataoka H. 2008. Numerical simulations of a wind-induced vibrating square cylinder within turbulent boundary layer. *J. Wind Eng. Ind. Aerodyn.* 96:1985–97

Keating A, De Prisco G, Piomelli U. 2006. Interface conditions for hybrid RANS/LES calculations. *Int. J. Heat Fluid Flow* 27:4696–712

Keating A, Piomelli U, Balaras E, Kaltenbach HJ. 2004. A priori and a posteriori tests of inflow conditions for large-eddy simulation. *Phys. Fluids* 16:2623–39

Keck R-E, Mikkelsen R, Troldborg N, de Maré M, Hansen KS. 2014. Synthetic atmospheric turbulence and wind shear in large eddy simulations of wind turbine wakes. *Wind Energy* 17:1247–67

Kempf A, Klein M, Janicka J. 2005. Efficient generation of initial- and inflow-conditions for transient turbulent flows in arbitrary geometries. *Flow Turbul. Combust.* 74:67–84

Kempf A, Wysocki S, Pettit M. 2012. An efficient, parallel low-storage implementation of Klein's turbulence generator for LES and DNS. *Comput. Fluids* 60:58–60

Khujadze G, Oberlack M. 2004. DNS and scaling laws from new symmetry groups of ZPG turbulent boundary layer flow. *Theor. Comput. Fluid Dyn.* 18:391–411

Kim JW, Haeri S. 2015. An advanced synthetic eddy method for the computation of aerofoil turbulence interaction noise. *J. Comput. Phys.* 287:1–17

Kim Y, Castro IP, Xie Z. 2013. Divergence-free turbulent inflow conditions for large eddy simulations with incompressible flow solvers. *Comput. Fluids* 84:56–68

Klein M, Sadiki A, Janicka J. 2003. A digital filter based generation of inflow data for spatially developing direct numerical or large eddy simulations. *J. Comput. Phys.* 186:652–65

Knight DD. 2006. *Inflow boundary conditions for DNS and LES of compressible turbulent boundary layers*. Presented at AIAA Aerosp. Sci. Meet. Exhib., 44th, Reno, NV, AIAA Pap. 2006-498

Kondo K, Murakami S, Mochida A. 1997. Generation of velocity fluctuations for inflow boundary condition of LES. *J. Wind Eng. Ind. Aerodyn.* 67–68:51–64

Kong H, Choi H, Lee JS. 2000. Direct numerical simulation of turbulent thermal boundary layers. *Phys. Fluids* 12:2555–68

Kornev N, Hassel E. 2007. Method of random spots for generation of synthetic inhomogeneous turbulent fields with prescribed autocorrelation functions. *Commun. Numer. Methods Eng.* 23:35–43

Kraichnan RH. 1970. Diffusion by a random velocity field. *Phys. Fluids* 13:22–31

Lagha M, Kim J, Eldredge JD, Zhong X. 2011. A numerical study of compressible turbulent boundary layers. *Phys. Fluids* 23:015106

Laraufie R, Deck S, Sagaut P. 2011. A dynamic forcing method for unsteady turbulent inflow conditions. *J. Comput. Phys.* 230:8647–63

Larsson J. 2009. Blending technique for compressible inflow turbulence: algorithm localization and accuracy assessment. *J. Comput. Phys.* 228:933–37

Le H, Moin P. 1994. *Direct numerical simulation of turbulent flow over a backward-facing step*. Rep. TF-58, Thermosci. Div., Dep. Mech. Eng., Stanford Univ., Stanford, CA

Le H, Moin P, Kim J. 1997. Direct numerical simulation of turbulent flow over a backward-facing step. *J. Fluid Mech.* 330:349–74

Lee JH, Sung HJ. 2011a. Direct numerical simulation of a turbulent boundary layer up to $Re_\theta = 2500$. *Int. J. Heat Fluid Flow* 32:1–10

Lee JH, Sung HJ. 2011b. Very-large-scale motions in a turbulent boundary layer. *J. Fluid Mech.* 673:80–120

Lee S, Lele SK, Moin P. 1992. Simulation of spatially evolving turbulence and the applicability of Taylor's hypothesis in compressible flow. *Phys. Fluids A* 4:1521–30

Lee S, Lele SK, Moin P. 1993. Direct numerical simulation of isotropic turbulence interacting with a weak shock wave. *J. Fluid Mech.* 251:533–62

Lee SH, Sung HJ. 2007. Direct numerical simulation of the turbulent boundary layer over a rod-roughened wall. *J. Fluid Mech.* 584:125–46

Li Q, Coleman GN. 2004. DNS of an oblique shock wave impinging upon a turbulent boundary layer. In *Direct and Large-Eddy Simulation V*, ed. R Friedrich, BJ Geurts, O Métais, pp. 387–96. New York: Springer

Li YC, Cheng CM, Lo YL, Fang FM, Zheng DQ. 2015. Simulation of turbulent flows around a prism in suburban terrain inflow based on random flow generation method simulation. *J. Wind Eng. Ind. Aerodyn.* 146:51–58

Liu K, Pletcher RH. 2006. Inflow conditions for the large eddy simulation of turbulent boundary layers: a dynamic recycling procedure. *J. Comput. Phys.* 219:1–6

Lund T, Moin P. 1996. Large eddy simulation of a concave wall boundary layer. *Int. J. Heat Fluid Flow* 17:290–95

Lund T, Wu X, Squires KD. 1998. Generation of turbulent inflow data for spatially-developing boundary layer simulations. *J. Comput. Phys.* 140:233–58

Mahesh K, Lele SK, Moin P. 1997. The influence of entropy fluctuations on the interaction of turbulence with a shock wave. *J. Fluid Mech.* 334:353–79

Marusic I, Perry AE. 1995. A wall-wake model for the turbulence structure of boundary layers. Part 2. Further experimental support. *J. Fluid Mech.* 298:389–407

Maruyama T, Rodi W, Maruyama Y, Hiraoka H. 1999. Large eddy simulation of the turbulent boundary layer behind roughness elements using an artificially generated inflow. *J. Wind Eng. Ind. Aerodyn.* 83:381–92

Maruyama R, Tamura T, Okuda Y, Ohashi M. 2012. LES of turbulent boundary layer for inflow generation using stereo PIV measurement data. *J. Wind Eng. Ind. Aerodyn.* 104–6:379–88

Maxey MR. 1987. The gravitational settling of aerosol particles in homogeneous turbulence and random flow fields. *J. Fluid Mech.* 174:441–65

Mayor SD, Spalart PR, Tripoli GJ. 2002. Application of a perturbation recycling method in the large-eddy simulation of a mesoscale convective internal boundary layer. *J. Atmos. Sci.* 59:2385–95

Mirocha J, Kosović B, Kirkil G. 2014. Resolved turbulence characteristics in large-eddy simulations nested within mesoscale simulations using the Weather Research and Forecasting model. *Mon. Weather Rev.* 142:806–31

Moin P, Kim J. 1982. Numerical investigation of turbulent channel flow. *J. Fluid Mech.* 118:341–77

Moin P, Mahesh K. 1998. Direct numerical simulation: a tool in turbulence research. *Annu. Rev. Fluid Mech.* 30:539–78

Morgan B, Duraisamy K, Lele SK. 2014. Large eddy simulation of a normal shock train in a constant area isolator. *AIAA J.* 52:539–58

Morgan B, Larsson J, Kawai S, Lele SK. 2011. Improving low-frequency characteristics of recycling/rescaling inflow turbulence generation. *AIAA J.* 49:582–97

Mullenix NJ, Gaitonde DV, Visbal MR. 2013. Spatially developing supersonic turbulent boundary layers with a body-force-based method. *AIAA J.* 51:1805–19

Munters W, Meneveau C, Meyers J. 2015. Shifted periodic boundary conditions for simulations of wall-bounded turbulent flows. *Phys. Fluids* 28:025112

Muñoz-Esparza D, Kosović B, van Beeck J, Mirocha J. 2015. A stochastic perturbation method to generate inflow turbulence in large eddy simulation models: application to neutrally stratified atmospheric boundary layers. *Phys. Fluids* 27:035102

Na Y, Moin P. 1998. Direct numerical simulation of a separated turbulent boundary layer. *J. Fluid Mech.* 374:379–405

Nakayama H, Takemi T, Nagai H. 2012. Large-eddy simulation of urban boundary-layer flows by generating turbulent inflows from mesoscale meteorological simulations. *Atmos. Sci. Lett.* 13:180–86

Nikitin N. 2007. Spatial periodicity of spatially evolving turbulent flow caused by inflow boundary condition. *Phys. Fluids* 19:091703

Nozawa K, Tamura T. 2002. Large eddy simulation of the flow around a low-rise building immersed in a rough-wall turbulent boundary layer. *J. Wind Eng. Ind. Aerodyn.* 90:1151–62

Pamiès M, Weiss PÉ, Garnier E, Deck S, Sagaut P. 2009. Generation of synthetic turbulent inflow data for large eddy simulation of spatially evolving wall-bounded flows. *Phys. Fluids* 21:045103

Park SB, Baik JJ, Lee SH. 2015. Impacts of mesoscale wind on turbulent flow and ventilation in a densely build-up urban area. *J. Appl. Meteorol. Climatol.* 54:811–24

Perret L, Delville J, Manceau R, Bonnet JP. 2006. Generation of turbulent inflow conditions for large-eddy simulation from stereoscopic PIV measurements. *Int. J. Heat Fluid Flow* 27:576–84

Perret L, Delville J, Manceau R, Bonnet JP. 2008. Turbulent inflow conditions for large-eddy simulation based on low-order empirical model. *Phys. Fluids* 20:075107

Perry AE, Chong MS. 1982. On the mechanism of wall turbulence. *J. Fluid Mech.* 119:173–217

Pierce CD, Moin P. 1998. Method for generating equilibrium swirling inflow conditions. *AIAA J.* 36:1325–27

Pierce CD, Moin P. 2004. Progress-variable approach for large-eddy simulation of non-premixed turbulent combustion. *J. Fluid Mech.* 504:73–97

Pirozzoli S, Bernardini M. 2011. Direct numerical simulation database for impinging shock wave/turbulent boundary-layer interaction. *AIAA J.* 49:1307–12

Pirozzoli S, Bernardini M. 2013. Probing high Reynolds number effects in numerical boundary layers. *Phys. Fluids* 25:021704

Pirozzoli S, Grasso F, Gatski TB. 2004. Direct numerical simulation and analysis of a spatially evolving supersonic turbulent boundary layer at $M = 2.25$. *Phys. Fluids* 16:530–45

Poletto R, Craft T, Revell A. 2013. A new divergence free synthetic–eddy method for the reproduction of inlet flow conditions for LES. *Flow Turbul. Combust.* 91:519–39

Priebe S, Martin MP. 2010. *Low frequency unsteadiness in the DNS of a compression ramp shockwave and turbulent boundary layer interaction*. Presented at AIAA Aerosp. Sci. Meet., 48th, Orlando, FL, AIAA Pap. 2010-108

Rai MM, Moin P. 1993. Direct numerical simulation of transition and turbulence in a spatially evolving boundary layer. *J. Comput. Phys.* 109:169–92

Rai RK, Gopalan H, Naughton JW. 2016. Effects of spatial and temporal resolution of the turbulent inflow on wind turbine performance estimation. *Wind Energy*. In press. doi:10.1002/we.1888

Rogallo RS. 1981. *Numerical experiments in homogeneous turbulence*. Tech. Memo 81315, NASA Ames Res. Cent., Moffett Field, CA

Rogallo RS, Moin P. 1984. Numerical simulation of turbulent flows. *Annu. Rev. Fluid Mech.* 16:99–137

Roidl B, Meinke M, Schröder W. 2013. A reformulated synthetic turbulence generation method for a zonal RANS-LES method and its application to zero-pressure gradient boundary layers. *Int. J. Heat Fluid Flow* 44:28–40

Roussel C, Alizard F, Grasso F. 2015. *Turbulence generation and sensitivity to mean inflow conditions for a supersonic flow in a rectangular duct at* $M = 1.61$. Presented at AIAA Comput. Fluid Dyn. Conf., 22nd, Dallas, TX, AIAA Pap. 2015-2618

Sagaut P, Garnier E, Tromeur E, Larchevêque L, Labourasse E. 2004. Turbulent inflow conditions for large-eddy simulation of compressible wall-bounded flows. *AIAA J.* 42:469–77

Saghafian A, Shunn L, Philips DA, Ham F. 2015. Large eddy simulations of the HIFiRE scramjet using a compressible flamelet/progress variable approach. *Proc. Combust. Inst.* 35:2163–72

Sandham ND, Yao YF, Lawal, AA. 2003. Large-eddy simulation of transonic turbulent flow over a bump. *Int. J. Heat Fluid Flow* 24:584–95

Sayadi T, Hamman CW, Moin P. 2013. Direct numerical simulation of complete H-type and K-type transitions with implications for the dynamics of turbulent boundary layers. *J. Fluid Mech.* 724:480–509

Schlatter P, Örlü R. 2010. Assessment of direct numerical simulation data of turbulent boundary layers. *J. Fluid Mech.* 659:116–26

Schlatter P, Örlü R. 2012. Turbulent boundary layers at moderate Reynolds numbers: inflow length and tripping effects. *J. Fluid Mech.* 710:5–34

Schlüter JU, Pitsch H, Moin P. 2004. Large-eddy simulation inflow conditions for coupling with Reynolds-averaged flow solvers. *AIAA J.* 42:478–84

Schlüter JU, Wu X, Kim S, Shankaran S, Alonso JJ, Pitsch H. 2005. A framework for coupling Reynolds-averaged with large-eddy simulations for gas turbine applications. *ASME J. Fluids Eng.* 127:806–15

Schmidt S, Breuer M. 2015. Extended synthetic turbulent inflow generator within a hybrid LES URANS methodology for the prediction of non-equilibrium wall bounded flows. *Flow Turbul. Combust.* 95:669–707

Shur ML, Spalart PR, Strelets MK, Travin AK. 2014. Synthetic turbulence generators for RANS LES interfaces in zonal simulations of aerodynamic and aeroacoustic problems. *Flow Turbul. Combust.* 93:63–92

Simens MP, Jiménez J, Hoyas S, Mizuno Y. 2009. A high-resolution code for turbulent boundary layers. *J. Comput. Phys.* 228:4218–31

Smirnov A, Shi S, Celik I. 2001. Random flow generation technique for large eddy simulations and particle-dynamics modeling. *ASME J. Fluids Eng.* 123:359–71

Smits A, Dussauge J-P. 1996. *Turbulent Shear Layers in Supersonic Flow*. Woodbury, NY: Am. Inst. Phys.

Spalart PR. 1988. Direct simulation of a turbulent boundary layer up to $Re_\theta = 1410$. *J. Fluid Mech.* 187:61–98

Spalart PR. 2009. Detached-eddy simulation. *Annu. Rev. Fluid Mech.* 41:181–202

Spalart PR, Strelets M, Travin A. 2006. Direct numerical simulation of large-eddy-break-up devices in a boundary layer. *Int. J. Heat Fluid Flow* 27:902–10

Spille-Kohoff A, Kaltenbach HJ. 2001. *Generation of turbulent inflow data with a prescribed shear-stress profile*. Compil. Part Notice ADP013648, Def. Tech. Inf. Cent., Fort Belvoir, VA

Stevens RJAM, Meneveau C. 2017. Wind-farm fluid mechanics and turbulence. *Annu. Rev. Fluid Mech.* 49:In press

Stolz S, Adams NA. 2003. Large-eddy simulation of high-Reynolds-number supersonic boundary layers using the approximate deconvolution model and a rescaling and recycling technique. *Phys. Fluids* 15:2398–412

Subbareddy P, Peterson D, Candler GV, Marusic I. 2006. *A synthetic inflow generation method using the attached eddy hypothesis*. Presented at AIAA Appl. Aerodyn. Conf., 24th, San Francisco, AIAA Pap. 2006-3672

Tabor GR, Baba-Ahmadi MH. 2010. Inlet conditions for large eddy simulation: a review. *Comput. Fluids* 39:553–67

Tamura T. 2008. Towards practical use of LES in wind engineering. *J. Wind Eng. Ind. Aerodyn.* 96:1451–71

Tamura T, Okuno A, Sugio Y. 2007. LES analysis of turbulent boundary layer over 3D steep hill covered with vegetation. *J. Wind Eng. Ind. Aerodyn.* 95:1463–75

Tamura T, Ono Y. 2003. LES analysis on aeroelastic instability of prisms in turbulent flow. *J. Wind Eng. Ind. Aerodyn.* 91:1827–46

Tomas JM, Pourquie MJBM, Jonker HJJ. 2015. The influence of an obstacle on flow and pollutant dispersion in neutral and stable boundary layers. *Atmos. Environ.* 113:236–46

Touber E, Sandham ND. 2009. Large-eddy simulation of low-frequency unsteadiness in a turbulent shock-induced separation bubble. *Theor. Comput. Fluid Dyn.* 23:79–107

Tyacke JC, Tucker PG. 2015. Future use of large eddy simulation in aero-engines. *J. Turbomach.* 137:081005

Urbin G, Knight D. 2001. Large-eddy simulation of a supersonic boundary layer using an unstructured grid. *AIAA J.* 39:1288–95

Veloudis I, Yang Z, McGuirk JJ, Page GJ, Spencer A. 2007. Novel implementation and assessment of a digital filter based approach for the generation of LES inlet conditions. *Flow Turbul. Combust.* 79:1–24

Wallace JM, Vukoslavčević PV. 2010. Measurement of the velocity gradient tensor in turbulent flows. *Annu. Rev. Fluid Mech.* 42:157–81

Westerweel J, Elsinga GE, Adrian RJ. 2013. Particle image velocimetry for complex turbulent flows. *Annu. Rev. Fluid Mech.* 45:409–36

Wu X. 2010. Establishing the generality of three phenomena using a boundary layer with freestream passing wakes. *J. Fluid Mech.* 664:193–219

Wu X, Hickey J-P. 2012. Visualization of continuous stream of grid turbulence past the Langston turbine cascade. *AIAA J.* 50:215–25

Wu X, Li LT, St. Hilaire M. 2009. Migration of a turbulent patch through a high-pressure turbine cascade. *Phys. Fluids* 21:025110

Wu X, Moin P. 2009. Direct numerical simulation of turbulence in a nominally-zero-pressure-gradient flat-plate boundary layer. *J. Fluid Mech.* 630:5–41

Wu X, Moin P, Adrian RJ, Baltzer JR. 2015. Osborne Reynolds pipe flow: direct simulation from laminar through gradual transition to fully developed turbulence. *PNAS* 112:7920–24

Wu X, Moin P, Hickey J-P. 2014. Boundary layer bypass transition. *Phys. Fluids* 26:091104

Wu X, Schlüter J, Moin P, Pitsch H, Iaccarino G, Ham F. 2006. Computational study on the internal layer in a diffuser. *J. Fluid Mech.* 550:391–412

Wu X, Squires KD. 1998. Numerical investigation of the turbulent boundary layer over a bump. *J. Fluid Mech.* 362:229–71

Wu X, Squires KD. 2000. Prediction and investigation of the turbulent flow over a rotating disk. *J. Fluid Mech.* 418:231–64

Wu X, Squires KD, Lund TS. 1995. Large eddy simulation of a spatially developing turbulent boundary layer. *Proc. IEEE/ACM Supercomput. Conf.*, p. 67. New York: IEEE

Xiao X, Edwards JR, Hassan HA, Baurle RA. 2003. Inflow boundary conditions for hybrid large eddy/Reynolds averaged Navier-Stokes simulations. *AIAA J.* 41:1481–89

Xie ZT, Castro IP. 2008. Efficient generation of inflow conditions for large eddy simulation of street-scale flows. *Flow Turbul. Combust.* 81:449–70

Xiong Z, Nagarajan S, Lele SK. 2004. Simple method for generating inflow turbulence. *AIAA J.* 42:2164–66

Xu S, Martin MP. 2004. Assessment of inflow boundary conditions for compressible turbulent boundary layers. *Phys. Fluids* 16:2623–39

Yan BW, Li QS. 2015. Inflow turbulence generation methods with large eddy simulation for wind effects on tall buildings. *Comput. Fluids* 116:158–75

Yang XIA, Meneveau C. 2015. Recycling inflow method for simulations of spatially evolving turbulent boundary layers over rough surfaces. *J. Turbul.* 17:75–93

Yu R, Bai XS. 2014. A fully divergence-free method for generation of inhomogeneous and anisotropic turbulence with large spatial variation. *J. Comput. Phys.* 256:234–53

Yuan J, Piomelli U. 2015. Numerical simulation of a spatially developing accelerating boundary layer over roughness. *J. Fluid Mech.* 780:192–214